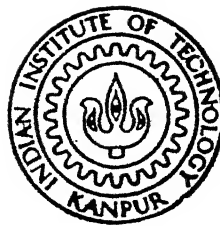


A FINITE ELEMENT BASED THERMAL ANALYSIS OF OPTIMAL RISER DESIGN FOR ALLOY CASTINGS

by

SAIBAL ROY CHOWDHURY



DEPARTMENT OF MECHANICAL ENGINEERING

INDIAN INSTITUTE OF TECHNOLOGY, KANPUR

OCTOBER, 1988

ME

1988

M

Th
621.471
C459f

CHO

FIN

A FINITE ELEMENT BASED THERMAL ANALYSIS OF OPTIMAL RISER DESIGN FOR ALLOY CASTINGS

A Thesis Submitted
In Partial Fulfilment of the Requirements
for the Degree of
MASTER OF TECHNOLOGY

by
SAIBAL ROY CHOWDHURY

to the
DEPARTMENT OF MECHANICAL ENGINEERING
INDIAN INSTITUTE OF TECHNOLOGY, KANPUR
OCTOBER, 1988

28 APR 1989
CENTRAL LIBRARY
U.S. AIR FORCE
Acc. No. A. 104226

ME-1988-M-CHO-FIN

CERTIFICATE



ii)

This is to certify that the thesis entitled, 'A FINITE ELEMENT BASED THERMAL ANALYSIS OF OPTIMAL RISER DESIGN FOR ALLOY CASTINGS' by SAIBAL ROY CHOWDHURY, is a bonafide record of the work done by him under our guidance and supervision, for the award of the Degree of Master of Technology at the Indian Institute of Technology, Kanpur. The work carried out in this thesis has not been submitted elsewhere for the award of a degree.

A handwritten signature in cursive script, likely belonging to Dr. T. Sundarajan.

(Dr. T. Sundarajan)
Assistant Professor
Department of Mechanical Engg.
I.I.T. Kanpur

A handwritten signature in cursive script, likely belonging to Dr. P.S. Ghoshdastidar.

(Dr. P.S. Ghoshdastidar)
Assistant Professor
Department of Mechanical Engg.
I.I.T. Kanpur

October, 1988.

ACKNOWLEDGEMENTS

It is with deep sense of gratitude, I acknowledge the guidance provided by Dr. T. Sundarajan and Dr. P.S. Ghoshdastidar. I shall remain indebted to them for their kind co-operation, valuable suggestions, timely guidance and above all, the inspiration they rendered to me throughout the development of the present investigation.

My sincerest thanks to all my friends for rendering me the timely help during my thesis work and making my stay here a memorable one.

Finally, I am grateful to my parents for the encouragement they have always give me.

October, 1988
I.I.T. Kanpur.

-Saibal Roy Chowdhury

CONTENTS

	<u>Page</u>
LIST OF TABLES	v)
LIST OF FIGURES	vi)
NOMENCLATURE	ix)
ABSTRACT	xi)
CHAPTER 1 INTRODUCTION	1
1.1 General Background	1
1.2 Literature Survey	2
1.3 Objectives of the Present Work	7
1.4 Organisation of the Present Work	8
CHAPTER 2 MATHEMATICAL MODELLING OF THE PROBLEM	9
2.1 Mechanism of Alloy Solidification	9
2.2 Temperature Distribution of Different Layers	11
2.3 Thermal Model for Alloy Solidification	15
2.4 Riser Design and Placement	19
2.5 Optimization of Riser Size and Dimension	27
CHAPTER 3 FINITE ELEMENT ANALYSIS	31
3.1 Introduction	31
3.2 Description of the FEM Solution Procedure by Galerkin Approach	32
3.3 Method of Weighted Residuals	34
3.4 FEM Solution Procedure to the Alloy Casting Problem	36
3.5 Matrix Solution Procedure	45
CHAPTER 4 RESULTS AND DISCUSSIONS	49
4.1 Solidification Analysis	49
4.2 Riser Design and Placement	50
4.2.1 Choice of Riser Size	50
4.2.2 Riser Placement and Optimal Riser Design Parameters	52
4.3 Feeding Distance	53
CHAPTER 5 CONCLUSIONS AND SUGGESTIONS	66
5.1 Conclusions	66
5.2 Suggestions for Future Work	66
REFERENCES	67

LIST OF TABLES

<u>Table No.</u>	<u>Title</u>	<u>Page</u>
2.1	Thermal Properties of Aluminium Alloy, Steel, Sand Mould and Sand-base.	29
2.2	Typical Constants for Steel Castings.	30
2.3	Calculation Conditions.	30

LIST OF FIGURES

<u>Fig. No.</u>	<u>Title</u>	<u>Page</u>
2.1	Equilibrium phase diagram of A-B alloy	12
2.2	Development of columnar crystals	12
2.3	Variation of concentration of B with distance from mould face	13
2.4	Dendritic crystal growth structure	13
2.5	Temperature distribution in different layers	14
2.6	Geometry of the problem	16
2.7	Proper combinations of volume and freezing ratios of steel	25
3.1	Finite element mesh for solution domain	33
3.2	Parabolic eight noded element showing typical node numbering and associated discrete variables. For programming anticlockwise sequence is used	42
3.3	Typical shape function variation for an eight noded isoparametric element	42
3.4	Definition of front and element numbering for minimum front width	48
4.1	Solidification of a bar casting, of Aluminium alloy (92.5% Al, 3% Cu, 4.5% Si)	55

<u>Fig. No.</u>	<u>Title</u>	<u>Page</u>
4.2	Solidification of a bar casting of 0.15% carbon steel for convective heat loss from the boundary. No centreline shrinkage area when bar of length twice the maximum feeding distance of riser	56
4.3	Solidification of a bar casting of 0.15% carbon steel for convective and radiative heat loss from the boundary	57
4.4	Risering of a cube casting of Aluminium alloy (92.5% Al, 3% Cu, 4.5% Ni). Proportionate riser used	58
4.5	Risering of a cube casting of Aluminium alloy (92.5% Al, 3% Cu, 4.5% Ni). Disproportionate riser used	59
4.6	Risering of a cubic casting of Aluminium alloy (92.5% Al, 3% Cu, 4.5% Ni). Modified optimum riser used.	60
4.7	Risering of a dumbbell shaped casting of Aluminium alloy (92.5% Al, 3% Cu, 4.5% Ni) with two risers, one at each end of the casting Isolated liquid region seen	61
4.8	Risering of a dumbbell shaped casting of Aluminium alloy (92.5% Al, 3% Cu, 4.5% Ni) with two risers one each at the centre of each casting. Isolated liquid region seen.	62

<u>Fig. No.</u>	<u>Title</u>	<u>Page</u>
4.9	Risering of a dumbbell shaped casting of Aluminium alloy (92.5% Al, 3% Cu, 4.5% Ni). Two proportionate risers one each at the centre of each casting. No isolated liquid region.	63
4.10	Solidification of a bar casting of 0.15% carbon steel. Centreline shrinkage areas seen when bar length greater than twice the maximum feeding distance	64
4.11	Comparison of present result with typical risering curve.	65

NOMENCLATURE

C_p	Specific heat
K	Thermal conductivity
h_c	Convective heat transfer coefficient
h_r	Radiative heat transfer coefficient
N_i and N_j	Shape function for the 8-noded isoparametric element
q	H/D ratio; where H = height of riser and D = dia of riser
Q	Rate of heat generation per unit volume
A_c	Surface area of casting
V_c	Volume of casting
T	Temperature to be calculated
T_{amb}	Ambient fluid temperature
T_{init}	Initial temperature of the fluid (or melt)
T_f	Temperature of fluid
t	Time
Δt	Time step
x, y	Co-ordinates
i, j	Indices corresponding to a node
M_R	Riser modulus
M_c	Casting modulus.

Greek Symbols

ρ	Density in kg/m^3
σ	Stefan Boltzman constant
ε	Emissivity
ξ, η	Local coordinates
θ	Fraction of implicit differencing for time discretization

Subscripts and Superscripts

e	Pertaining to an element
D	For the whole domain
f	Fluid (air).

ABSTRACT

A finite element based two dimensional transient heat transfer analysis has been performed to model the solidification of steel and aluminium alloy castings. The work has been to arrive at optimal riser design criteria based on the solidification process modelling.

The heat transfer formulation is based on heat conduction through the phases. The natural convective flow inside the liquid region has been neglected for the sake of simplicity. The heat release due to phase change in the solidifying mushy region is accounted through modified specific heat of the metal in the temperature range of solidification.

Eight noded isoparametric elements have been used for discretizing the solution domain. Quadratic interpolation for temperature has been employed within each element. Generalized heat transfer boundary conditions of natural convective or radiative heat loss to the environment and heat conduction loss into the sand-base have been included. The transient temperature variation has been obtained by marching in time using an implicit finite difference procedure.

Based on the temperature results of the FEM analysis, isotherms were plotted within the casting at different times. From this the formation of isolated liquid regions which are cut-off from the riser are identified. If any such regions are

predicted within the given casting configuration, the casting is termed unsound. Using this technique the optimality of riser dimensions and riser placement have been investigated for chunky and bar castings of steel and aluminium alloy. The results show good agreement with available classical works of riser design.

CHAPTER 1

INTRODUCTION

1.1 GENERAL BACKGROUND

Metal casting is an industry which involves high annual investment all over the world. An improvement in the quality of the castings and reducing the number of rejects would result in a large amount of saving for the casting industry.

For many years the production of sound castings was largely a matter of trial and error. In the early seventies, attention was focussed towards the scientific aspects of the production and design of castings. One such approach constituted the studies of the heat transfer mechanisms by which castings solidify and the rates at which solidification takes place. Of late, research of a more practical nature which is concerned with the design and placement of risers for castings has been carried out using modern computer simulation and graphical techniques. The present study deals with some of the practical aspects which need to be considered for the production of sound steel and aluminium alloy castings.

The physical process involved in alloy solidification are primarily thermal in origin. A basic knowledge of the thermal phenomena will be helpful in meeting the various design requirements in a scientific way. The present study is aimed at developing an appropriate thermal model of the solidification of

sand-mould castings of alloy metals. It is also intended to calculate the rate of solidification in the casting as a function of time and predict the occurrence of isolated liquid regions whose shrinkage due to solidification cannot be compensated by liquid fed from riser. By appropriately modifying the riser design, it is desired to eliminate casting defects such as shrinkage cavities with the help of the computer model.

1.2 LITERATURE SURVEY

Many investigators have contributed to the theoretical and experimental investigations on alloy solidification within a casting, over the past two decades. With regard to riser design, simplistic models exist which have led to the establishment of the current practices in the casting industry. However, very precise estimates of the riser dimensions and locations are not possible through these analyses. Limited work is also available on computer aided design of risers using modern simulation and graphical techniques. Here a brief survey of the available literature on alloy solidification and riser design is presented.

Classical analytical solutions were derived by Neumann and Stefan for the propagation of a one-dimensional solidification front through a semi-infinite medium (1) considering only heat conduction within the solid and liquid phases. These solutions have been extended for a linear variation of thermal conductivity and for including radiative heat transfer in the

medium by (2,3) . Effects of buoyancy driven flow upon the rate of solidification have been considered by (4,5) for simple geometries, using the finite difference solution technique. These works have the limitation that they are not applicable for complex geometries and boundary conditions for which the solidification front may not be planar.

Ostrach and Kroger (6) have considered the role of natural convection in the analysis of the steady state phase change associated with the continuous casting. While the work mentioned above concentrates on the effects of fluid motion an attempt to study the exact nature of the fluid motion itself has been made by Szekely and Stanek(7) . But the energy equation they considered did not contain any velocity terms. Hence the heat transfer process is not affected by buoyancy, conduction was the only transport phenomenon.

Sparrow, Patankar and Ramadani (8) carried out the analysis for two dimensional melting in a cylindrical enclosure taking natural convection into account. Their results were much different from those of the earlier conduction based solutions. Ramachandran, Gupta and Jaluria (9) studied the solidification in an enclosed region with natural convection in the melt for various heat transfer boundary conditions. They used an alternating direction implicit finite difference technique along with successive relaxation.

Jaisuk Yoo and Rubinsky (10) , have analysed the two dimensional solidification process with natural convection in

the melt, using FEM. Similar to Ramachandran, Gupta and Jaluria (9), they considered a simple rectangular enclosure. They solved the governing equations using a novel "front tracking" Finite Element Method for predicting the interface movement.

J.A. Sekhar, S. Kou and R. Mehrabian (11) considered a model for the stationary transient heat flow problem during rapid melting and solidification of an alloy with a mushy zone in which the heat of fusion is absorbed and liberated over a range of temperatures. A one-dimensional heat flow model which accounts for the heat of fusion was recently proposed by Hsu et al (12). This model employs the approximate integral technique coupled with the numerical technique developed by Murray and Landis (13) for the melting and solidification of a pure metal.

As regards the conventional practice of computing the optimal size of riser that will feed a given casting the methods adopted in the casting industry are largely based on the pioneering works of Chvorinov (14), Caine (15), Bishop (16) and Merchant (17).

According to Chvorinov (14) the freezing time of a casting is governed by its $(V/A)^2$ ratio, where V is the volume and A is the surface area of the casting. Once $(V/A)^2$ ratio of the casting is computed, the $(V/A)^2$ ratio of the riser is selected such that it is a little larger

(about 20%) than that of the casting so that the riser solidifies later. Caine (15) , who used Chvorinov's relation, defined a new term called relative freezing time, which is the ratio of $(A/V)^2$ ratio of casting to $(A/V)^2$ ratio of riser. Considering the shape variable, Bishop (16) restated the Chvorinov's rule and presented a curve of $(L+W)/T$ vs. the ratio of the riser volume to the casting volume, which relates the length, width and thickness of a sound casting to its freezing ratio. Based on these works Merchant (17) proposed a general equation for riser size calculations. Although, these methods give reliable results they are time consuming. Large errors are likely to occur with complicated castings (since the effective surface area of castings which contain edges and corners is substantially different from the real area). Also detailed information on the shrinkage cavity size and its location are not available from solutions based on the above methods.

However, in recent times, the F.E.M. simulation technique has considerably simplified and improved the casting design procedures. Prasanna Kumar et al (18) have attempted F.E.M. formulations of 1-D freeze wave without assuming freeze wave equations, and a further extension of the model to a 2-D situation. The basic F.E.M. procedure to determine solidification times has been formulated using 2-D heat transfer conditions.

In their papers, Imafuku and Chijiwa (19,20) have presented a method which predicts the shapes of shrinkage

cavities and porosities in steel castings with sand moulds. The method is analytically formulated in terms of the functions of solid fraction and shrinkage cavity ratio, by means of mass conservation law. A close agreement between the results of the experiment and the calculations with regard to both temperature and shrinkage cavities have been demonstrated.

The work done by Abis (21) describes the use of computer methods to obtain a good description of the solidification pattern in an aluminium casting and has been tested by means of a numerical/experimental work on a 3-D mould-metal system. A FEM simulation adopting non-moving mesh was used to calculate the transient thermal field during the phase transition.

Recently G.L. Shekar (22) has considered the interactive graphics approach coupled with the Finite Element simulation for predicting the occurrence of cavities inside an alloy casting for a two-dimensional situation. He demonstrated the validity of his technique by comparing with the known empirical results of the risering practice for castings of standard shapes. However the heat transfer boundary conditions in Shekar's work were not generalized for the sake of simplicity.

In the present work, an approach similar to that of Shekar has been considered with more realistic heat transfer boundary conditions on the external boundary of the

casting. Also, a computer software has been developed using 8-noded isoparametric curvilinear elements which are capable of providing more accurate solutions for the temperature field and can handle complex geometries, while in the work of Shekar less accurate 3-noded triangular elements were used. Further the present approach is more suitable for the inclusion of buoyancy-driven flow effects from solidification point of view.

1.3 OBJECTIVES OF THE PRESENT WORK

The present study deals with alloy solidification within a sand mould with appropriate heat transfer boundary conditions. The main objective is to determine the riser size and location for producing sound castings thereby eliminating the costly trial and error method.

The FEM solution technique is used to solve the 2-D transient heat transfer equation. From the predictions of the analysis, the solidification process within both the casting and the riser can be visualized by plotting the isotherms at different times in a graph paper. From these patterns the isolated liquid regions which cannot be fed for shrinkage compensation from the view can be observed. If isolated regions are identified then the size of shrinkage cavities can also be predicted. Once the occurrence of isolated regions is identified, it can be eliminated by changing the size or location of the riser(s) thereby achieving sound

castings. Thus, an optional riser design through detailed heat transfer analysis for an alloy casting is the objective of the present work.

1.4 ORGANISATION OF THE PRESENT WORK

The mathematical modelling of the problem has been dealt in Chapter 2. The problem description, the assumptions made and the governing equations are discussed in this chapter. The FEM formulation has been dealt with in Chapter 3. The results and discussions have been made in Chapter 4 which summarises the study conducted on both chunky and bar castings. Conclusions and suggestions for future work are covered in Chapter 5.

CHAPTER 2

MATHEMATICAL MODELLING OF THE PROBLEM

A clear understanding of the mechanism of solidification and cooling of liquid metals and alloys is essential for the production of sound castings. During alloy solidification, many important characteristics such as the crystal structure and the alloy composition at different parts of the casting are decided. Moreover, unless a proper care is taken defects like shrinkage cavities will occur. Here we shall briefly discuss the salient features of the process of alloy solidification.

2.1 MECHANISM OF ALLOY SOLIDIFICATION

An alloy, unlike a pure metal, does not have a sharply defined freezing temperature. Instead, it takes place over a range of temperatures. During the process, the solid phases separating out at different temperatures possess varying compositions. Due to all these facts, the direction of crystal growth in an alloy depends on various factors, such as

- (i) the composition gradient within the casting,
- (ii) the variation of solidus temperature with composition,
and
- (iii) the thermal gradients within the mould.

Each of these factors are discussed by considering the example of a solid solution alloy whose phase diagram is shown in Fig. 2.1.

Let the liquid alloy have the composition C_0 (of B in A). Also let T_f be the freezing point of pure metal A, and T_L and T_S , respectively the liquidus and solidus temperatures (the upper and lower limits for the solidification range) for the alloy of composition C_0 . As the liquid alloy is cooled down to temperature T_L , solid starts to separate out. The concentration of B in these solids is only C_1 (C_0) as is evident from the Fig. 2.1. As a result, the concentration of B in the liquid, near the solid liquid interface, increases to a value more than C_0 . Figure 2.3 shows this for the situation where the solidification front has progressed up to some distant d from the mould face.

Now, considering two points P and Q within the liquid alloy, P being just beyond the solid-liquid interface as indicated in Fig. 2.3. The solidus temperatures corresponding to the compositions at P and Q are T_P and T_Q , respectively (see Fig. 2.1). Let T'_P and T'_Q be the actual temperatures at the points P and Q. T'_Q is greater than T'_P due to the thermal gradient within the casting. If both T'_Q and T'_P lie in the range T_P to T_Q , then the liquid at Q is supercooled, whereas that at P is not. This implies that crystallization starts at Q sooner than at P. If this difference is very prominent, the columnar growth of crystals (See Fig. 2.2) starting from

the mould surface is hampered which is undesirable. The crystal growth in such a situation appears as in (Fig. 2.4). Thus a dendritic crystal structure is produced. If the crystallization at Q gets completed before it starts at P (due to a very small thermal gradient) then randomly-oriented crystals may appear inside the casting. Moreover, the presence of solid crystals ahead of the solid-liquid interface makes feeding of the liquid metal more difficult. This also implies greater risk of having voids within the casting.

2.2 TEMPERATURE DISTRIBUTION OF DIFFERENT LAYERS WITHIN THE CASTING

The heat rejected by the liquid metal is dissipated through the mould wall. The heat, released as a result of cooling and solidification of the liquid metal, passes through different layers. The temperature distribution in these layers, at any instant, is schematically shown in Fig. 2.5. The thermal resistances which governs the entire solidification process are those of the liquid, mushy, solidified region, the metal-mould interface, the mold, and the ambient air. These six different regions are indicated by numbers 1 to 6 in Fig. 2.5. A detailed heat transfer analysis is required to predict the variation of temperature through various layers and the formulation of such a thermal model is described below.

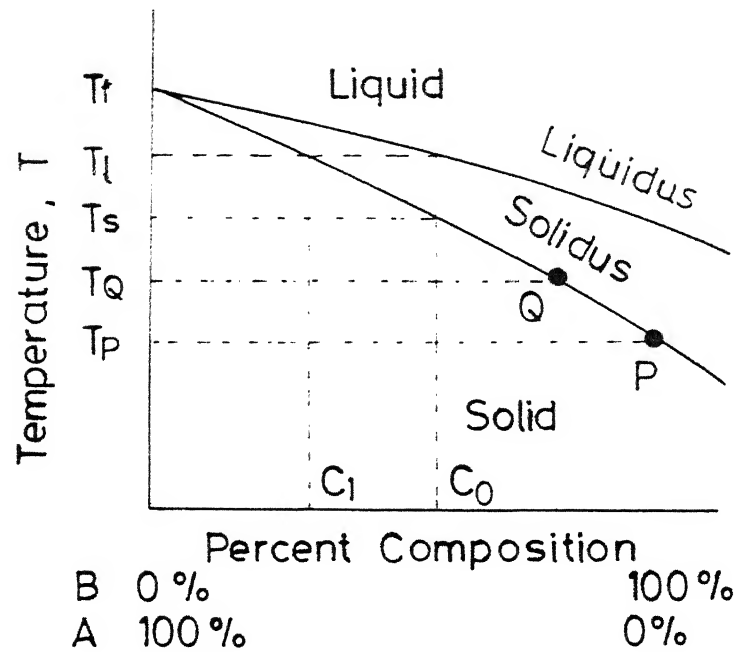


Fig 2.1 Equilibrium Phase Diagram of A - B Alloy.

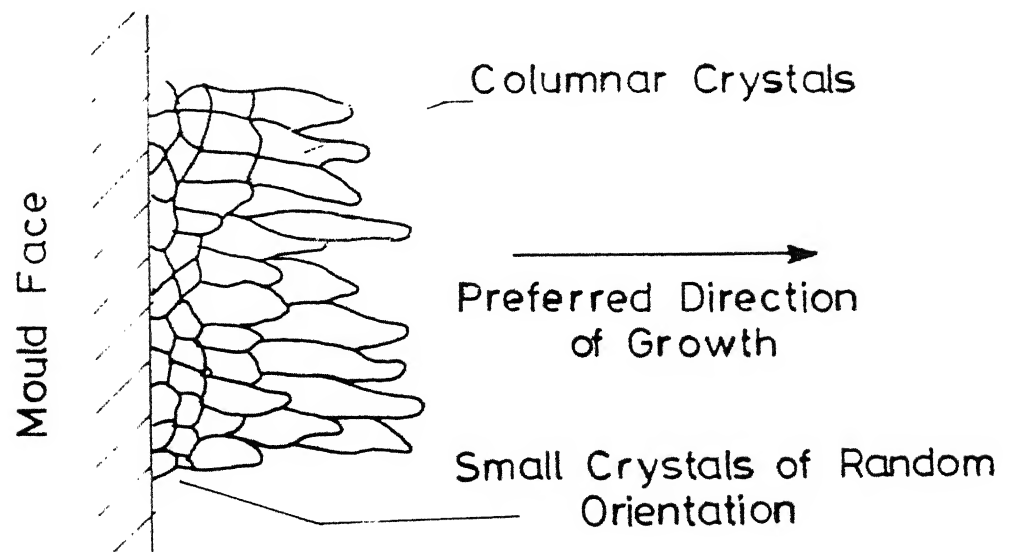


Fig. 2.2 Development of Columnar Crystals.

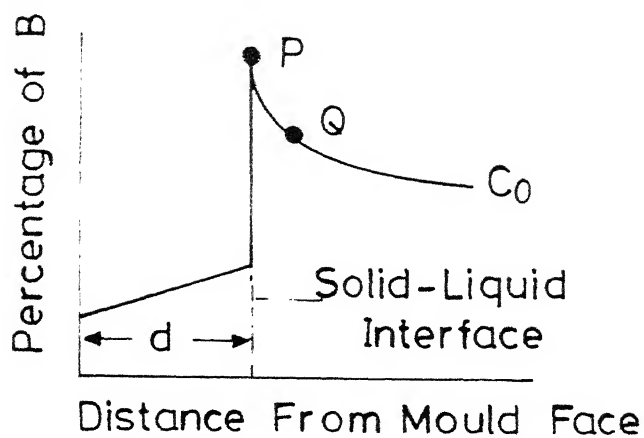


Fig. 2.3 Variation of Concentration of B with Distance from mould Face.

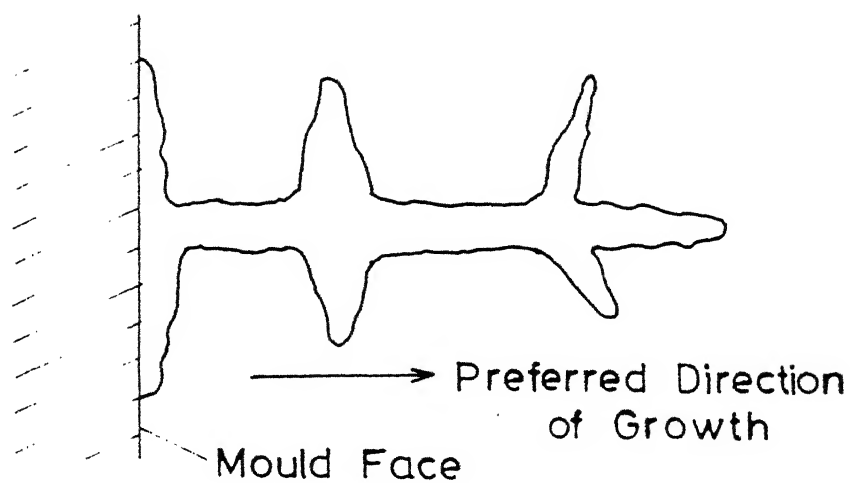


Fig. 2.4 Dendritic Crystal Growth Structure.

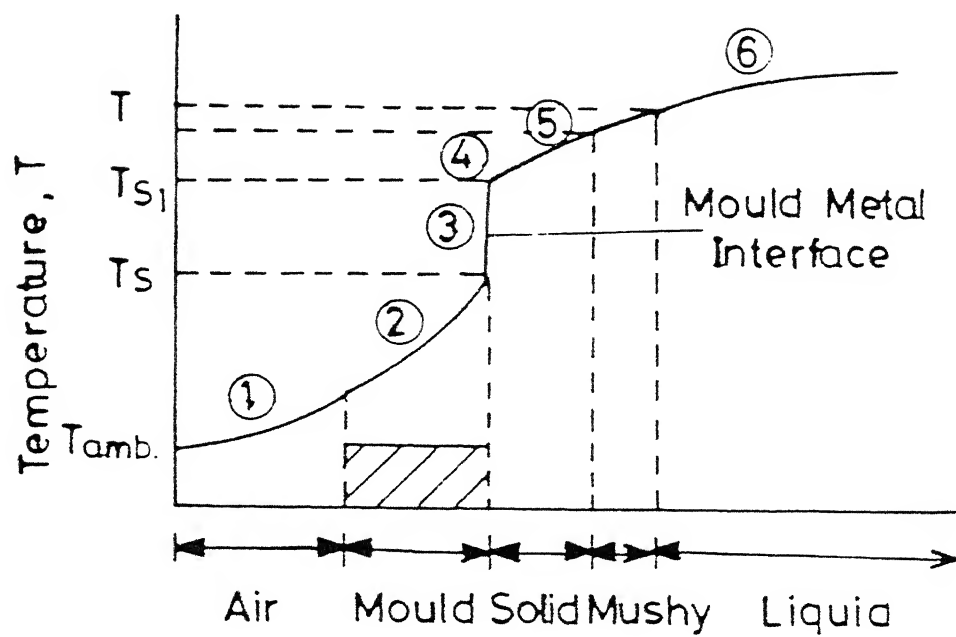


Fig. 25 Temperature Distribution in Different Layers.

2.3 THERMAL MODEL FOR ALLOY SOLIDIFICATION

A transient 2-D heat flow model is developed for alloy solidification with a mushy zone in which the latent heat is absorbed over a wide range of temperatures. The equations and solution methodology developed are general enough to be applicable to a variety of other solidification processing problems. A 2-D situation has been modelled for the sake of simplicity.

The geometry of the sand mould, casting and the sand-base on which the heat transfer analysis has been performed is shown in Fig. 2.6. The boundaries of the solution domain are subjected to different modes of heat transfer conditions such as convective heat transfer, specified temperature and in some cases radiative heat transfer. As a result of these boundaries conditions and heat dissipation from the melt, temperature gradients arise within the melt and the sand mould which leads to solidification of the liquid. As the solidification progresses, three distinct regions are observed, namely:

- (i) liquid
- (ii) mushy
- (iii) solid

These zones have different thermophysical properties. Typical values of the properties of these three phases for the steel and the aluminium alloy considered in the present work are listed in Table 2.1.

Boundary Conditions at Regions 1-10

1, 9, 10 - Constant Temperature ($T_{amb.}$)

2, 3, 4, 6, 7, 8 - Radiation/Convection

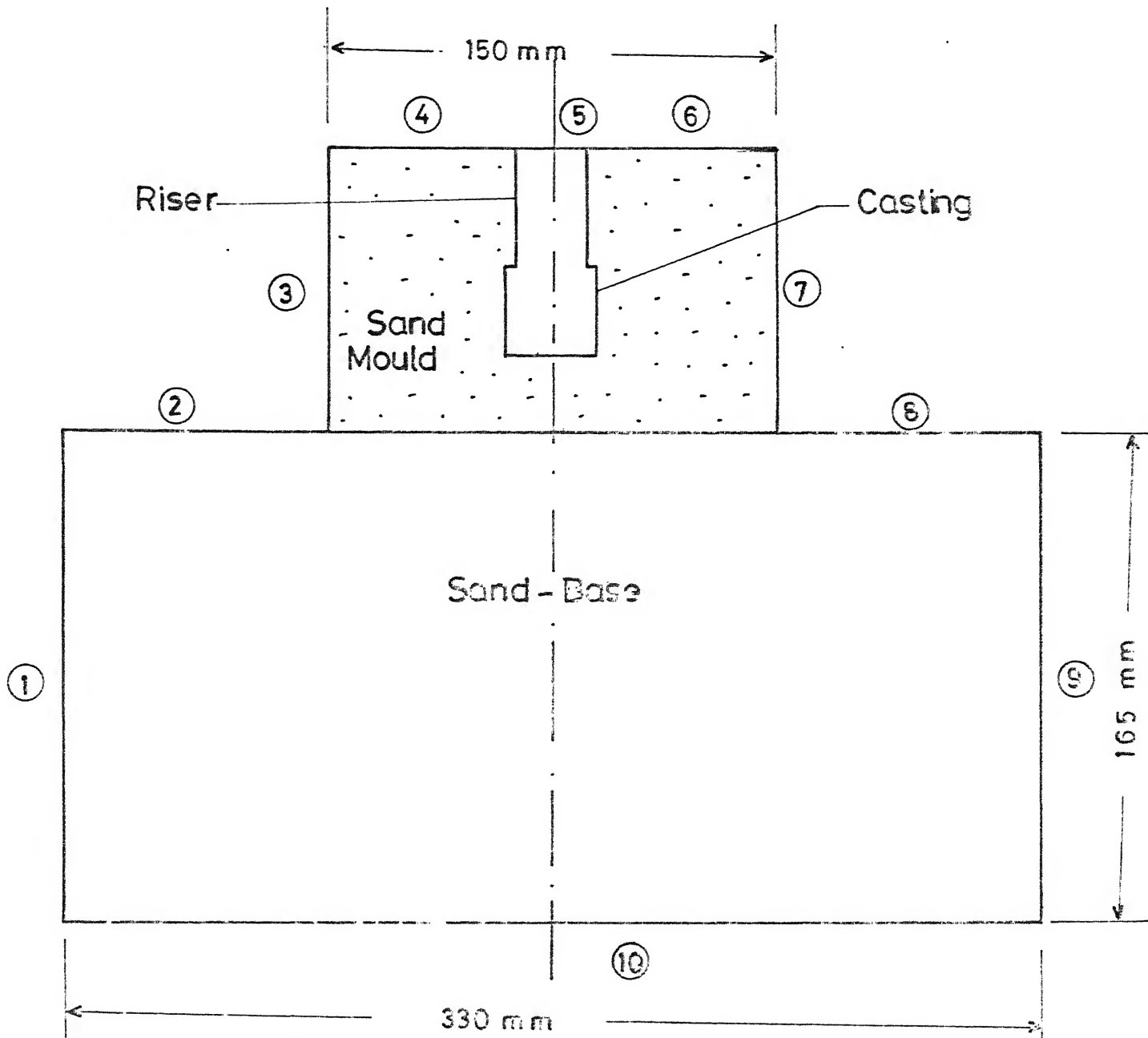


Fig.2.6 Geometry of the Problem.

Initially the molten alloy is considered to be at a temperature greater than its melting temperature. This additional heat above that necessary for melting is called superheat. This superheat is necessary to provide the fluidity to the liquid while pouring and it allows the melt to be transferred into the mould freely. Thus the melt can access all the locations within the mould without starting to freeze even after coming into contact with the cold wall of the mould.

The main assumptions that have been invoked in the present investigation are:

- (a) The density, conductivity and heat capacity of the solid, mushy and liquid regions are independent of temperatures but different from each other.⁺
- (b) For the mushy region an average thermal conductivity and a high heat capacity (due to latent heat) are used.⁺
- (c) The effect of natural convection in the liquid zone is neglected as the rate of heat transfer is enhanced only by a small factor.
- (d) It is assumed that the sand mould is kept on a very large sand base. The sides and bottom of the sand base are assumed to be at room temperature. The top surfaces of the sand base and the mould along with the sides of the mould are subjected to natural convective heat loss.

+ These assumptions are not very realistic during alloy solidification since the solid and liquid fractions are not throughout the mushy region. However, the major effects of property variation are still accounted for, by the consideration of average properties for each phase.

- (e) The melt poured into the mould has a prescribed degree of superheat.

With these assumptions the 2-D transient heat transfer equation governing the alloy solidification process is given by:

$$\rho_i c_{p_i} \frac{\partial T_i}{\partial t} = K_i \left[\frac{\partial^2 T_i}{\partial x^2} + \frac{\partial^2 T_i}{\partial y^2} \right] \quad (2.1)$$

where the suffix 'i' denotes different phases such as liquid, mushy, solid and mould. The above equation (2.1) is solved subject to the following boundary conditions:

- (i) On the surfaces 2, 3, 4, 5, 6, 7 and 8 (Refer Fig. 2.6) where convective heat loss occurs

$$h_c (T - T_f) = -K \frac{\partial T}{\partial x} \quad \text{for } t \geq 0 \quad (2.2a)$$

- (ii) For temperature specified boundaries 1, 9 and 10

$$T = T_{\text{amb}} \quad \text{for } t \geq 0 \quad (2.2b)$$

- (iii) On surface 5, insulated boundary conditions is used since the top surface of the riser is sprinkled with some exothermic powder to prevent heat losses through it. Therefore, for this boundary

$$\frac{\partial T}{\partial n} = 0 \quad (2.2c)$$

- (iv) The case where both convective and radiative boundary conditions are specified on the surfaces 2,3,4,6,7 and 8.

$$(h_r + h_c)(T - T_f) = -K \frac{\partial T}{\partial n} \text{ for } t \geq 0 \quad (2.2d)$$

where

$$h_r = \sigma \epsilon (T + T_f)(T^2 + T_f^2)$$

The initial conditions are:

- (a) $T = T_{init}$ at $t = 0$ within the casting and the riser (2.2e)
- (b) $T = T_{amb}$ at $t = 0$ in the sand mould and the sand base (2.2f)

For castings of various shapes placed inside sand moulds, the heat transfer analysis is carried out numerically within the entire region of the casting, mould and sand-base shown in Fig. 2.6. After obtaining the temperature field as a function of time from such an analysis it is linked to the optimal riser design as described in the next section.

2.4 RISER DESIGN AND PLACEMENT

When risering a casting, it is necessary to design a riser with sufficient dimensions so that it will be the last portion to solidify and thereby contain enough liquid metal to supply the shrinkage demand of the casting. Here, the conventional risering techniques are briefly discussed.

To properly determine the riser requirements of any casting the solidification characteristics of that casting must be evaluated. First, maximum feeding distances are calculated to determine riser locations. This can be done via the empirical rules (6) for the maximum feeding distance. Then the solidification time and the shrinkage volume of both the casting and the riser should be considered.

The solidification time of a given casting is commonly evaluated using the solidification modulus approach. The solidification modulus M_c of a casting is the ratio of the casting's volume to cooling surface area. Thus,

$$M_c = \frac{V_c}{A_c} \quad (2.3)$$

According to Chvorinov's Rule (14) ,

$$t = (K M_c)^2 \quad (2.4)$$

where

t = solidification time of the casting

K = constant of proportionality (mould constant).

Therefore, shapes having equal moduli have same solidification time when cast against the same molding medium.

To produce a shrinkage free casting the riser is designed to have a larger modulus than the casting it is required to feed. This is to ensure that the riser solidifies after the casting. In practice,

$$M_R = 1.2 M_c \quad (2.5)$$

The 20% compensation factor is necessary because of the nature of riser solidification. During the solidification process the riser is constantly losing volume and increasing its top cooling surface area. Therefore the riser modulus decreases on solidification. Upon the completion of solidification the residual riser modulus should not be lower than the casting modulus in order to get a sound casting.

The information on the amount of molten alloy needed from the riser is used only to compensate for the shrinkage that takes place from the pouring time till solidification is completed. Depending on the alloy, the percentage of this shrinkage varies from 2.5 to 7.5. Thus, the use of a large riser volume (to ensure large solidification time) is uneconomical. So, a riser should be designed with minimum possible volume while maintaining a cooling rate slower than that of the casting.

The riser is designed to have a low surface-to-volume ratio than that of the section it is to feed. The low ratio will reduce heat dissipation and hence the riser will remain liquid than an equal mass with large surface. For this purpose, a sphere is the ideal shape, but a sphere is difficult

to produce with a proper positioning in relation to the casting. It is more common to use a cylindrical shape that has a diameter larger than the part to be fed and a height equal to about one to one-half times the diameter.

In the present study the riser equations are obtained from Ref. (17) and it is used to get an approximate initial guess value of the riser diameter.

The riser equation is expressed as follows:

$$\frac{25(4q + 1)}{A_c} = \frac{q D}{s V_c} - \frac{1.275}{D^2} \quad (2.6)$$

An optimum value of q ($= H/D$) has to be chosen to calculate the value of D from Eqn. (2.6). The H/D ratio of the most compact cylinder which has a minimum surface area for a given volume can be determined in the following way:

$$A = \pi D H + 2 \left(\frac{\pi}{4}\right) D^2, \text{ and}$$

$$V = \frac{\pi}{4} D^2 H \text{ or } H = \frac{4V}{\pi D^2}$$

Hence,

$$A = \pi D \frac{4V}{\pi D^2} + 2\left(\frac{\pi}{4}\right) D^2 = \frac{4V}{D} + \left(\frac{\pi}{2}\right) D^2$$

For A to be minimum,

$$\frac{\partial A}{\partial D} = 0 \text{ or } -\frac{4V}{D^2} + \pi D = 0 \text{ or } D^3 = \frac{4V}{\pi}.$$

Again,

$$\frac{4V}{\pi} = D^2 H = D^3$$

or $H = D$ (2.7)

This shows that the optimum ratio of H/D is equal to 1 for a cylindrical riser. Equation (2.6) is also dependent on the percentage volumetric shrinkage along with H/D ratio. Two cases have been considered in the present study corresponding to that of an aluminium-alloy and steel.

(A) Initial Riser Size Calculations for an Aluminium Alloy

Percent volumetric shrinkage of aluminium alloy = 6.6.

(i) $H/D = 1$

Using the above values in Eqn. (2.6) we get

$$D^3 A_c - 8.25 D^2 V_c - 0.08415 V_c A_c = 0 \quad (2.8a)$$

(ii) $H/D = 1.33$

Putting the above values in Eqn. (2.6) gives

$$D^3 A_c - 7.8375 D^2 V_c - 0.06311 V_c A_c = 0 \quad (2.8b)$$

(iii) $H/D = 2$

Using the above values Eqn. (2.6) can be written as

$$D^3 A_c - 7.425 D^2 V_c - 0.042075 V_c A_c = 0 \quad (2.8c)$$

(B) Initial Riser Size Calculations for Steel

Percent volumetric shrinkage of steel = 3.0

(i) $H/D = 1$

Putting the above values in Eqn. (2.6) gives

$$D^3 A_c - 3.75 D^2 V_c - 0.03825 V_c A_c = 0 \quad (2.8d)$$

(ii) $H/D = 1.33$

Putting the above values in Eqn. (2.6) gives

$$D^3 A_c - 1.3125 D^2 V_c - 0.0286 V_c A_c = 0 \quad (2.8e)$$

To check the adequacy of the riser size for steel castings Caine's relationship was also used. It is known that solidification time is proportional to the square of the ratio/surface area. Caine's relationship, however, is based on the assumption that the cooling rate is linearly proportional to the surface area/volume. A typical risering curve for steel is depicted in Fig. 2.7. Here the ordinate of a point in the curve shows the volume ratio and the abscissa the freezing ratio and the subscripts c and r refer to the casting and the riser, respectively. For a given casting-riser combination if the point in Fig. 2.7 falls to the right of the curve, the size of the riser is adequate. The equation for a risering curve is of the form

$$x = \frac{a}{y-b} + c$$

where

a = freezing constant of the metal

b = the contraction ratio from liquid to solid

c = a constant depending on the different media around the riser and the casting.

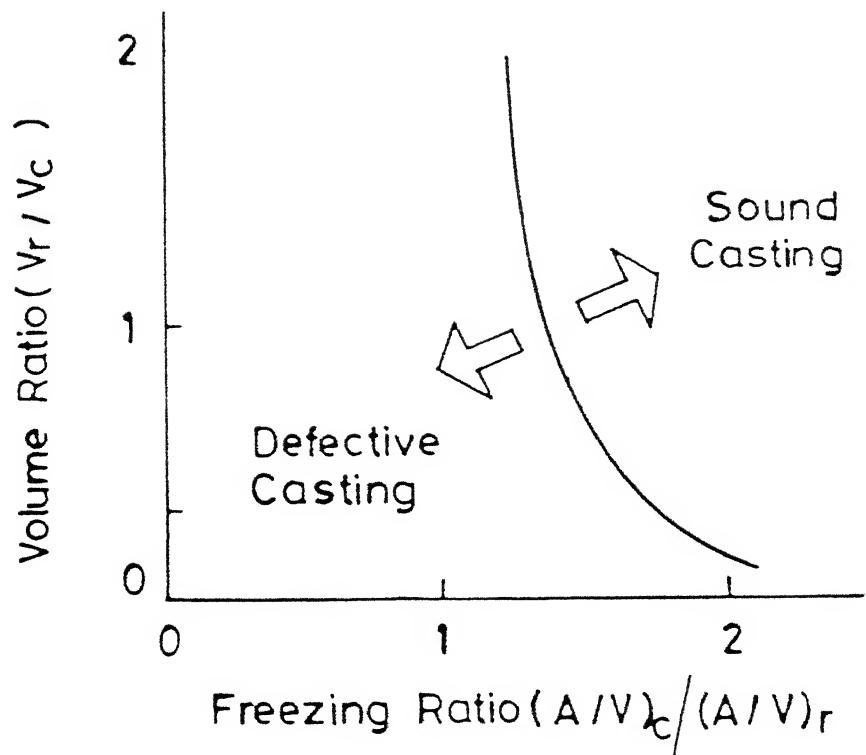


Fig. 2.7 Proper Combinations of Volume and Freezing Ratios for Steel.

Typical values of these constants for steel casting are given in Table (2.2).

So far our discussion has been restricted to the adequacy of the riser size from the points of view of shrinkage and cooling rate. Another important aspect of risering is to ensure that the available liquid metal in the riser can be fed to the desired locations within the casting. In fact the thermal gradient, within the casting, during the last stage of cooling is the most important factor which controls the occurrence of casting defects. The minimum allowable gradient depends on the shape and size of the cross-section. Generally one central riser is satisfactory if,

$$(i) \quad F_{\max} = 4.5 t \quad \text{for steel plates} \quad (2.9)$$

where 't' is the thickness of the plate

$$(ii) \quad F_{\max} = 6\sqrt{t} \quad \text{for steel bars} \quad (2.10)$$

where 't' is the thickness of the bar in cm.

The feeding distance should be measured from the edge of the riser. If the feeding distance is not proper centre line shrinkage will occur and hence the casting obtained will be unsound.

The problem of riser design and placement under consideration was solved with the help of FEM technique starting with an initial guess for the riser as given by the above calculations.

As the solidification proceeds with time it is checked whether any isolated liquid region is formed within the casting which will result in shrinkage cavities. In case such a region is found, the riser size is changed until it vanishes. Optimization of riser dimensions is carried out along with a search for the optimum placement of the riser such that no shrinkage defect occurs. Aluminium alloy and steel castings having a simple geometry such as bar or cube have been considered for convenience, although complex shapes can also be handled by this model easily.

2.5 OPTIMIZATION OF RISER SIZE AND DIMENSION

The use of a riser of small volume than that required to feed a casting leads to shrinkage cavity. The use of a riser with a very large volume (to ensure long solidification time) is also uneconomical from the cost point of view. Hence a riser should be designed with minimum possible volume while maintaining a cooling rate slower than that of the casting.

So initially to start with it was assumed that $H/D = 1$ and the diameter of the base of the riser was taken to be half the diameter of the casting base. In all the cases shrinkage cavities were obtained. The next step was to increase the riser size and this process was continued until all the isolated liquid regions disappeared from the casting.

It was observed that the optimal riser diameter was less as compared to the riser diameter calculated with the help of equation (2.6). Thus, overdesign of the riser can be avoided using the present computer model.

TABLE 2.1 : THERMAL PROPERTIES OF ALUMINIUM ALLOY,
STEEL, SAND MOULD AND SAND-BASE

	State	Thermal conductivity (W/m ⁰ C)	Specific Heat (J/kg ⁰ C)	Density (kg/m ³)
ALUMINIUM ALLOY (Al-3Cu-4,5Si)	SOLID	193.53	1162.04	2690
	LIQUID	91.96	1254.00	2560
	MUSHY	142.12	5095.42	2625
STEEL	SOLID	31.00	802.56	7500
	LIQUID	41.80	836.00	7000
	MUSHY	36.34	42636.00	7250
SAND MOULD	-	0.7524	1065.90	1580
SAND-BASE	-	0.3254	794.96	1500

TABLE 2.2 : TYPICAL CONSTANTS FOR STEEL CASTINGS

Freezing Constant (a)	Contraction Ratio (b)	(c)
0.10	0.03	1.00

TABLE 2.3 : CALCULATION CONDITIONS

Alloy	Liquidus Temp.(°C)	Solidus Temp.(°C)	Heat Trans. Coeffi- cient (W/m ² °C)	Ambient Temp. (°C)	Melt Temp. (°C)	Time Step (Sec.)	Sand-base Bottom Temp. (°C)
Alumi- nium	625	525	5-8	30	675	20	30
Steel	1525	1515	10-15	30	1700	20	30

CHAPTER 3

FINITE ELEMENT ANALYSIS

3.1 INTRODUCTION

The solution procedure that has been adopted for the problem under study is the Finite Element Method (FEM). Some of the most important advantages are the easy handling of complex geometrical shape of the solution domain and the general manner in which the boundary conditions are introduced. Rather than requiring every trial solution to satisfy the boundary condition the boundary conditions may be applied after obtaining the algebraic equations for the assemblage. Since the boundary conditions do not enter into equations for the individual elements, one can use the same field variable model for both internal and boundary elements. Moreover the field variables need not be changed, when the boundary conditions are changed. In addition FEM is also successful in representing complicated material property variations that are difficult to incorporate in other numerical methods. FEM also provides a systematic procedure for the derivation of the weighting function for problems with non-linearity and arbitrary domain. In view of the above mentioned generality and flexibility provided by FEM solution technique, it has been employed to solve the present problem.

3.2 DESCRIPTION OF THE FEM SOLUTION PROCEDURE BY GALERKIN'S APPROACH

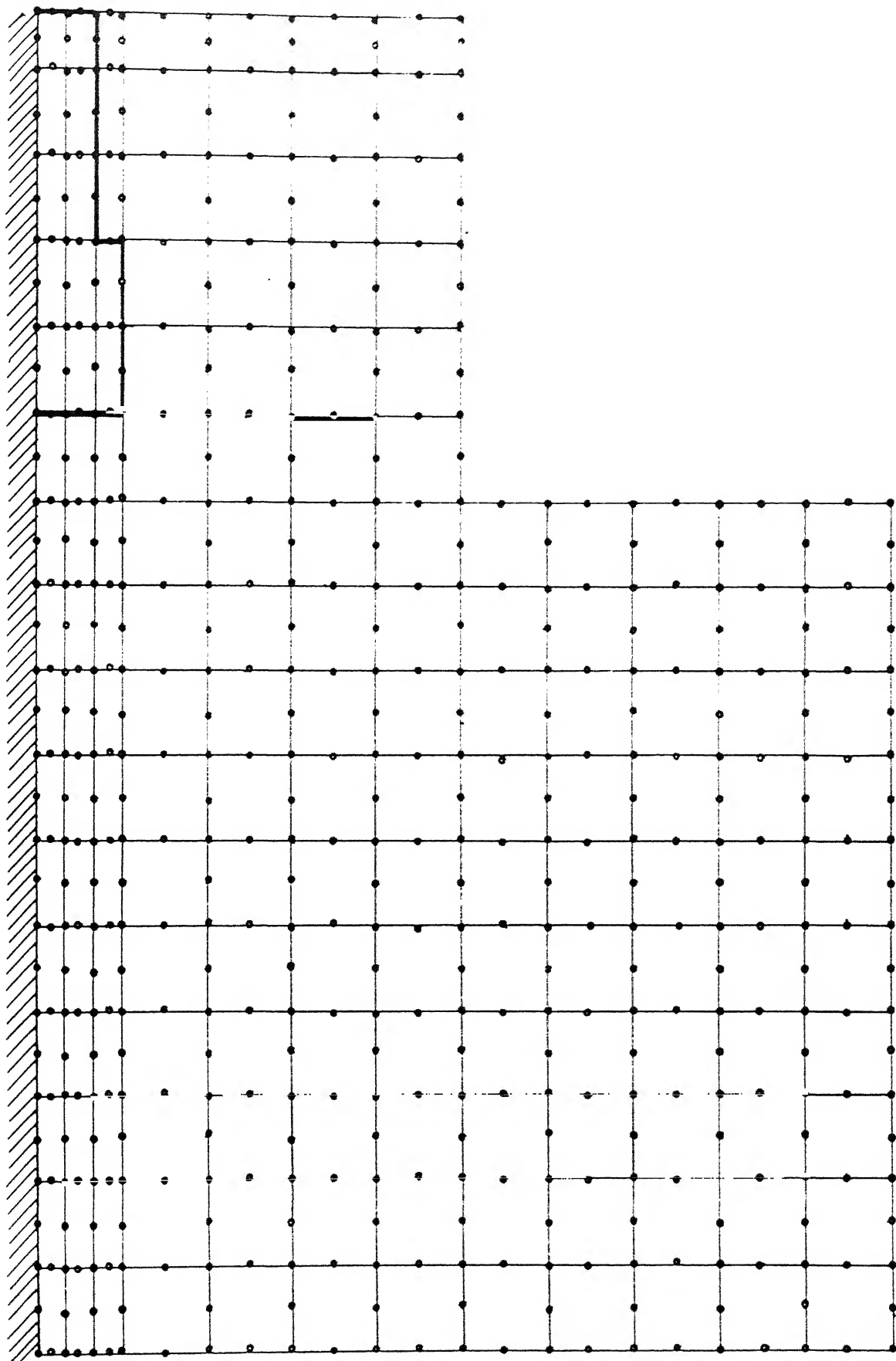
In FEM, the governing differential equations are converted into an equivalent set of integral equations which are minimized in some sense over the whole solution domain. The solution domain is divided into several small elements of known shape and the solution variable is approximated within each of these elements by suitable approximating functions. The integral governing equations are then evaluated within each element using the approximating functions and all such elemental integrals are assembled to obtain the final matrix equation to be solved. The above steps can be summed up as follows:

(a) Obtain the equivalent integral equations for describing the problem. The boundary conditions of the problem would be transformed into appropriate boundary integrals.

(b) Divide the solution domain into several elements and place chosen number of nodes within each element. Obtain the approximating functions for describing the field variable, within each element in terms of nodal values. A mesh-generation program may be used to obtain the finite element mesh

Fig. 3.1 .

(c) Each governing integral equation over the entire solution domain is written as the sum of the integral over all



No. of Nodal Points = 411, No. of Elements = 120

Fig. 3.1 Finite Element Mesh for Solution Domain .

elements.

(d) A typical element is isolated and the approximating functions for describing the field variables are obtained within that element in terms of their nodal values. For this element, firstly, the elemental integrals are evaluated leading to the formation of an elemental coefficient matrix and elemental right hand side vector. Then the boundary integrals (if any) are evaluated to obtain the boundary coefficient matrix and the boundary right hand side vector. These elemental and boundary coefficient matrices are assembled for each element to obtain the final form of the elemental coefficient matrix. A similar operation is done for the elemental right hand side vector also.

(e) The elemental coefficient matrices are then assembled for all the elements, giving rise to a global coefficient matrix. The elemental right hand side vectors are also assembled leading to the formation of the global right hand side vector.

(f) The matrix equations obtained in the previous step are solved to find the unknown field variables at all nodes.

In the present work, the Finite element approximation based on the Galerkin Method has been adopted.

3.3 METHOD OF WEIGHTED RESIDUALS

Weighted residual methods are, in essence, numerical

techniques which can be used to solve a set of partial differential equations. The first step in the application of the weighted residual procedure is to assume that the unknown variable, ϕ , can be approximated over the whole domain by

$$\phi^* = \sum_{i=1}^n N_i \phi_i \quad (3.1)$$

where N_i are the interpolation functions described in terms of the spatial coordinates (X, Y) and ϕ_i are the values of ϕ at certain chosen locations.

Consider the equation:

$$\mathcal{L}(\phi) = 0 \quad (3.2)$$

where ϕ is the exact solution of the differential operator. An approximate solution, ϕ^* , given by eq. (3.1), gives rise to an error or residue R , while substituted into eq. (3.2), such that

$$R = \mathcal{L}(\phi^*)$$

In the weighted residual methods, R is minimised over the whole solution domain in the integral sense with a set of arbitrary 'weighting functions', W_i , such that over the whole domain, D ,

$$\int_D W_i R \, dD = 0 \quad (3.3)$$

where $i = 1, 2, \dots, n$.

If the number of unknown values of ϕ is n , then by using n linear independent weighting functions, enough equations can be generated to solve all the unknowns. The only limitation, at this stage, placed on W_i , is that they must be positive, single-valued and finite.

The Galerkin's Method is a very special case of the method of weighted residuals, where the weighting functions, (W_i) , are taken to be the same as the interpolation functions (N_i) , which are more commonly known as shape functions.

Therefore, for Galerkin's Method, the residue minimization equations can be written as:

$$\int_D N_i \mathcal{L}(\phi^*) dD = 0$$

where

$$\phi = \sum_{j=1}^n N_j \phi_j \quad (3.4)$$

3.4 FEM SOLUTION PROCEDURE TO THE ALLOY-CASTING PROBLEM

A major objective in a conduction analysis is to determine the temperature field in a medium resulting from conditions that are imposed on its boundaries. Once this temperature distribution is known it is possible to optimize the riser size.

The 2-D heat conduction equation is of the form

$$\rho C_p \frac{\partial T}{\partial t} = K \nabla^2 T + Q \quad (3.5)$$

assuming constant thermal conductivity. The heat generation term has been neglected. Therefore Eqn.(3.5) can be written as

$$\rho C_p \frac{\partial T}{\partial t} - K \nabla^2 T = 0 \quad (3.6)$$

The equation (3.6) will be satisfied if temperature T is exact. Let us assume an approximate value of temperature say T^* and putting it in equation (3.6) gives

$$\rho C_p \frac{\partial T^*}{\partial t} - K \nabla^2 T^* = R \quad (3.7)$$

where R is the residue due to the approximate solution T^* . The next step is to minimize the residue R over the whole domain D by Galerkin's method. This is done by choosing some weighting function say N_i which is also the shape function. This gives

$$\iint_D N_i R \, dx \, dy = [0] \quad (3.8)$$

Substituting the value of R from Eqn. (3.7) into Eqn. (3.8) gives

$$\iint_D N_i \left(\rho C_p \frac{\partial T^*}{\partial t} - K \nabla^2 T^* \right) dx \, dy = [0] \quad (3.9)$$

$$\rho C_p \iint_D N_i \frac{\partial T^*}{\partial t} dx dy - K \iint_D N_i \nabla^2 T^* dx dy = [0] \quad (3.10)$$

The unknown variable T^* can be expanded in terms of its nodal values and shape functions as:

$$T^* = \sum_{j=1}^n N_j T_j \quad (3.11)$$

where n is the number of nodes per element.

With the help of the weak formulation the order of the second term in Eqn. (3.10) is reduced

$$-K \iint_D N_i \nabla^2 T^* dx dy = K \iint_D (\underline{\nabla} N_i \cdot \underline{\nabla} T^* - \underline{\nabla} \cdot (N_i \underline{\nabla} T^*)) dx dy \quad (3.12)$$

According to the divergence theorem (for a 2-D case)

$$\iint_D (\underline{\nabla} \cdot \underline{F}) dx dy = \oint \underline{F} \cdot \underline{n} dl \quad (3.13)$$

The last term in equation (3.12) using divergence theorem becomes

$$K \iint_D \underline{\nabla} \cdot (N_i \underline{\nabla} T^*) dx dy = K \oint_B N_i \underline{\nabla} T^* \cdot \underline{n} dl$$

$$\text{or } K \iint_D \underline{\nabla} \cdot (N_i \underline{\nabla} T^*) dx dy = K \oint_B N_i (\underline{\nabla} T^* \cdot \underline{n}) dl \quad (3.14)$$

where B denotes boundary integral.

But $\nabla T^* \cdot n = \frac{\partial T^*}{\partial n}$ which is nothing but the normal derivative to the boundary

$$-K \iint_D N_i \nabla^2 T^* dx dy = K \iint_D \nabla N_i \cdot \nabla T^* dx dy - \int N_i \left(K \frac{\partial T^*}{\partial n} \right) dl \quad (3.15)$$

or

$$-K \iint_D N_i \nabla^2 T^* dx dy = K \iint_D \left(\frac{\partial N_i}{\partial x} \cdot \frac{\partial T^*}{\partial x} + \frac{\partial N_i}{\partial y} \cdot \frac{\partial T^*}{\partial y} \right) dx dy - \int N_i \left(K \frac{\partial T^*}{\partial n} \right) dl \quad (3.16)$$

The problem has provisions for including all types of boundary conditions.

$$-K \frac{\partial T^*}{\partial n} = q \text{ for heat flux boundary condition}$$

$$-K \frac{\partial T^*}{\partial n} = h_c (T^* - T_f) \text{ for a convective boundary condition}$$

$$-K \frac{\partial T^*}{\partial n} = h_r (T^* - T_f) \text{ for a radiative boundary condition}$$

$$\text{where } h_r = \epsilon \sigma (T^* + T_f) (T^{*2} + T_f^2)$$

In the present work, only symmetrical-shaped castings have been considered and therefore, it is sufficient to solve only half the problem. This is done by considering a domain as shown in Fig. (3.1) with the prescription of an insulated

boundary conditions on the plane of symmetry.

For a convective boundary condition, Eqn. (3.15) takes the form

$$\begin{aligned}
 -K \iint_D N_i \nabla^2 T^* dx dy = & K \iint_D \left(\frac{\partial N_i}{\partial x} \cdot \frac{\partial T^*}{\partial x} + \frac{\partial N_i}{\partial y} \cdot \frac{\partial T^*}{\partial y} \right) dx dy \\
 & + \int_C N_i h (T^* - T_f) dl \quad (3.17)
 \end{aligned}$$

where C denotes the boundary with convection. Substituting Eqn. (3.17) in Eqn. (3.10), we get the final equation of the entire domain as

$$\begin{aligned}
 \rho C_p \left[\iint_D N_i N_j dx dy \right] [\dot{T}_j] + K \left[\iint_D \left(\frac{\partial N_i}{\partial x} \cdot \frac{\partial N_j}{\partial x} + \frac{\partial N_i}{\partial y} \cdot \frac{\partial N_j}{\partial y} \right) dx dy \right] [T_j] \\
 + h \left[\int_C N_i N_j dl \right] [T_j] = h T_f \left[\int_C N_i dl \right] \quad (3.18)
 \end{aligned}$$

In the above equation, the summation has been dropped by adopting the convention that summation is implied if a subscript is repeated.

In the present study, 8-noded iso-parametric elements have been used (See Fig. 3.2). The term isoparametric implies that both the element geometry and the variation in the variable across the element are described utilising the same type of polynomial or shape function. The global coordinates (x,y) of a

point inside an element can thus be expressed in terms of nodal coordinates and shape functions as it has been done for the field variables. Therefore,

$$x = \sum_{i=1}^8 N_i x_i \quad (3.19)$$

$$y = \sum_{i=1}^8 N_i y_i \quad (3.20)$$

The shape functions N_i for the 8-noded isoparametric elements (Refer Fig. 3.3) in terms of local coordinates ξ and η , are given by the following relations.

For corner nodes:

$$N_i = \frac{1}{4} (1 + \xi_i \xi) (1 + \eta_i \eta) (\xi_i \xi + \eta_i \eta - 1) \quad (3.21)$$

For mid-nodes:

$$N_i = \frac{1}{2} (1 - \xi^2) (1 + \eta_i \eta) \text{ for } \xi_i = 0 \quad (3.22)$$

$$N_i = \frac{1}{2} (1 - \eta^2) (1 + \xi_i \xi) \text{ for } \eta_i = 0 \quad (3.23)$$

Substituting equations (3.19) - (3.23) in equation (3.18), the final form of the assembled matrix equations are:

$$[GMASS] [\dot{T}_j] + [GCON] [T_j] = [GGEN] \quad (3.24)$$

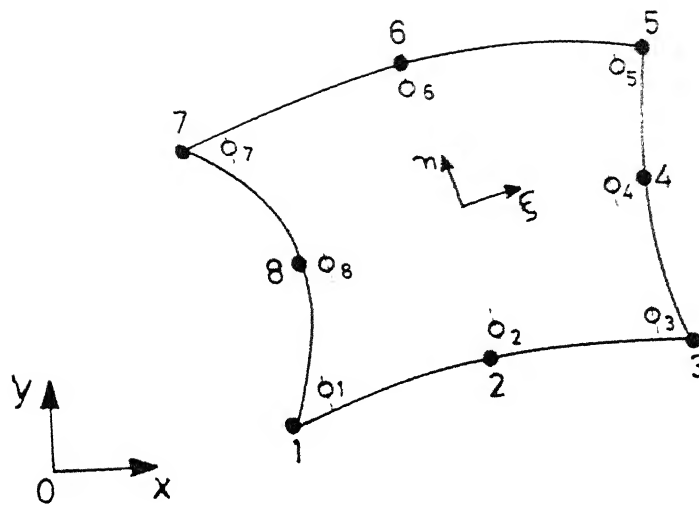


Fig. 3.2 Parabolic Eight Noded Element Showing Typical Node Numbering and Associated Discrete Variables. For Programming Anticlockwise Sequence is Used.

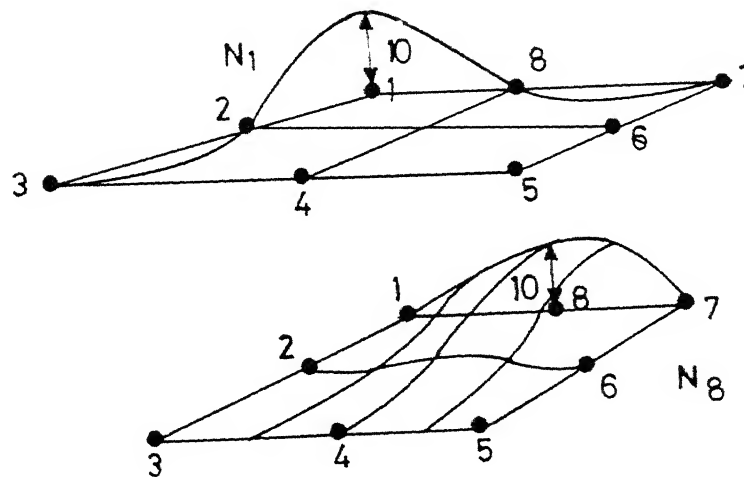


Fig. 3.3 Typical Shape Function Variation for an Eight Noded Isoparametric Element.

where

[GMASS] is the global transient matrix,

[GCON] is the global conductivity matrix,

[GGEN] is the global right hand side vector.

In terms of shape functions or their derivatives, these matrices and vector are expressed as:

$$GMASS = \sum_{e=1}^m \rho C_p \int \int_{(e)} N_i N_j dx dy \quad (3.25)$$

$$GCON = \sum_{e=1}^m \left[K \int \int_{(e)} \left(\frac{\partial N_i}{\partial x} \cdot \frac{\partial N_j}{\partial x} + \frac{\partial N_i}{\partial y} \cdot \frac{\partial N_j}{\partial y} \right) dx dy + h \int_{(e)} N_i N_j dl \right] \quad (3.26)$$

$$GGEN = \sum_{e=1}^m h T_f \int_{(e)} N_i dl \quad (3.27)$$

The equation (3.18) represents a set of simultaneous first-order ordinary differential equations of the variable T and its time derivatives.

Hence the finite difference technique has been adopted to approximate the time derivatives. This leads to the final matrix equations of the form:

$$[A] [T] = [C] \quad (3.28)$$

There are three major schemes for handling the time derivatives in the finite-difference technique, namely:

- (i) Implicit scheme
- (ii) Explicit scheme
- (iii) Crank-Nicholson scheme.

Applying a generalised scheme which considers a fraction of the explicit scheme and a fraction of the implicit scheme, Eqn. (3.24) can be rewritten as,

$$\begin{aligned}
 & \{ [GMASS + \theta \Delta t GCON] \} [T_j]^{K+1} \\
 & = \{ [GMASS - (1 - \theta) \Delta t GCON] \} [T_j]^K \\
 & + [GGEN] \Delta t
 \end{aligned} \tag{3.29}$$

The three schemes mentioned above can be obtained from Eqn. (3.29) by assuming different values of the fraction. For instance,

$$\begin{aligned}
 \theta &= 0 \text{ for explicit scheme} \\
 \theta &= 0.5 \text{ for Crank-Nicholson scheme} \\
 \theta &= 1.0 \text{ for implicit scheme.}
 \end{aligned}$$

Since the implicit scheme is the most stable one and has no restriction as far as the time step is concerned, it has been used in the present study.

For implicit scheme, Equation (3.29) simplifies to the form:

$$\begin{aligned}
 & \{ [GMASS] + \Delta t [GCON] \} [T_j]^{K+1} \\
 & = [GMASS] [T_j]^K + [GGEN] \Delta t
 \end{aligned} \tag{3.30}$$

Equation (3.30) can be solved to obtain the temperature vector at the $(K+1)$ th time level, knowing the temperature vector at the K th time level.

3.5 MATRIX SOLUTION PROCEDURE:

Here the Frontal solution method has been used to solve the assembled matrix equations. It is a well-known fact that the method adopted for solving the assembled matrix equation has a significant bearing on the computer storage requirement and execution time when the total number of unknown variables is very large. It becomes very time consuming and the core memory problem is very acute when a large number of unknowns are solved by the matrix inversion technique. The Frontal solution technique can handle quite a large number of variables without the problem of large core memory and the computer execution time is also quite less.

The Frontal solution technique used in the present work is based on the direct Gaussian elimination procedure for solving the symmetric matrices where the leading diagonal is always used as a pivot. For unsymmetric matrices encountered in a wide range of engineering problems, the most suitable pivot is not necessarily on the leading diagonal and a Frontal solution routine exists for off diagonal pivoting (23) . But since this tends to be more time consuming, the method used in the present work uses only diagonal pivoting and incorporates many features of the Frontal method for solving symmetric matrices.

The overall Frontal solution technique covers the following steps:

- i) Formation of the elemental matrices.
- ii) Assembling into a small, temporary global matrix of chosen size.
- iii) Introduction of known variable boundary condition.
- iv) Reduction of the global matrix using Gaussian elimination procedure.
- v) Back substitution.

The primary objective of the Frontal method is the elimination of variables as soon as possible after their introduction, via appropriate equations, into the global matrix. When the contributions from all the elements to a particular node point have been assembled, the corresponding variables associated with that node can be eliminated. The complete matrix is, therefore, never assembled, since the reduced equations can be eliminated from the core and stored on disc. The equations held in core, with the corresponding nodes and variables, are termed as the FRONT and the number of unknown variables in the front is termed as the FRONT WIDTH.

The Front width changes continuously, since, if the nodal matrix contribution have been fully summed the corresponding equation reduction based on the diagonal pivot can be executed.

For a non-symmetric global matrix, a preassigned global matrix core area is filled from contributing elements, the largest diagonal entry in the pre-assigned core is then found and used as the pivot in a direct Gaussian elimination process. As the maximum, predetermined number of equations are eliminated, the corresponding reduced equations are written on to disc and more elements and corresponding equations are taken into core.

The equations, nodes and variables currently in core are termed active, those assigned to disc as deactivated and those yet to appear in core as inactive. This is shown diagrammatically in Fig. (3.4).

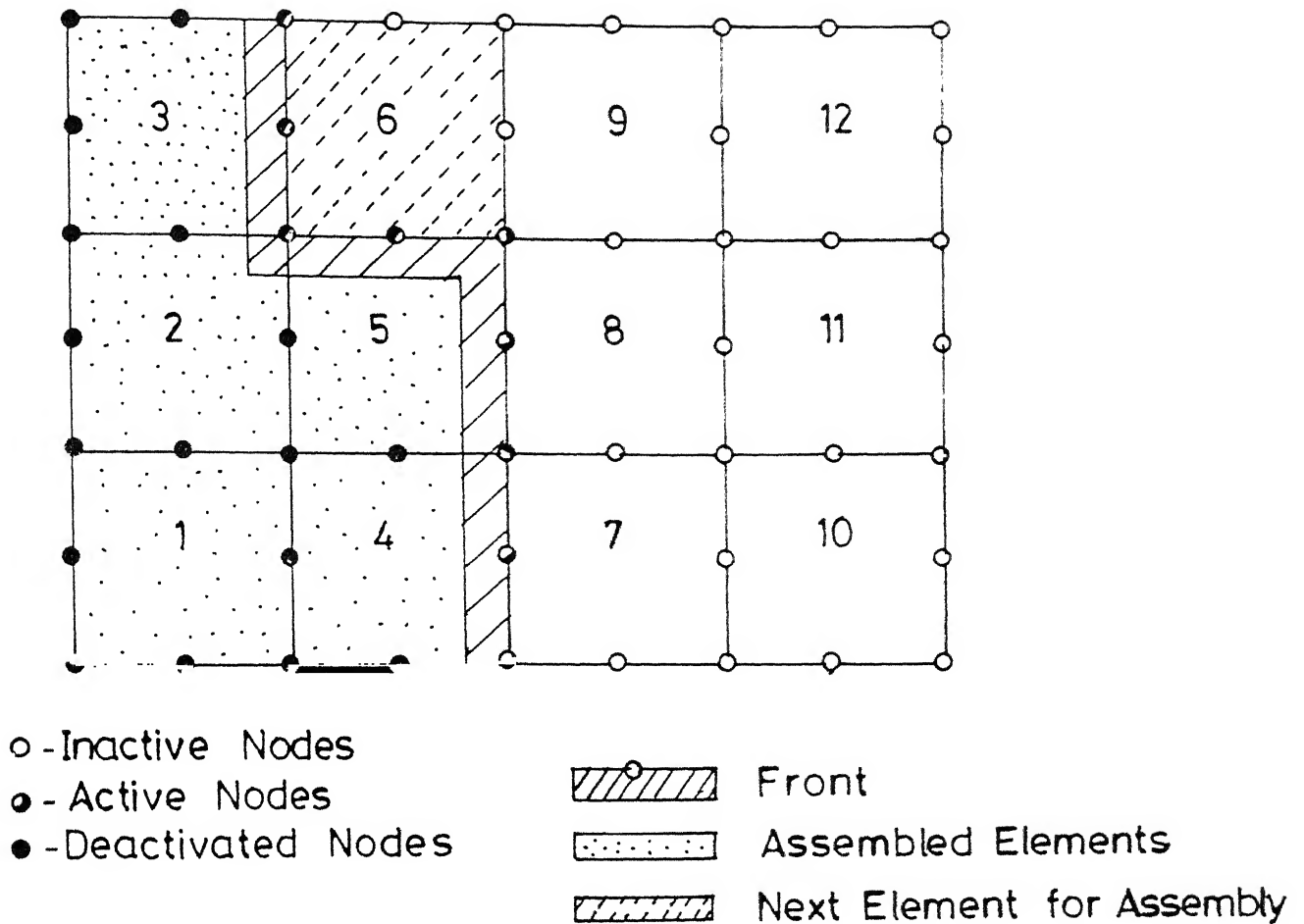


Fig.3.4 Definition of Front and Element Numbering for Minimum Front Width.

CHAPTER 4

RESULTS AND DISCUSSIONS

Results of the temperature field have been obtained for various casting and riser configurations using the FEM technique. The isotherms have been plotted to identify the zones of isolated liquid regions which lead to the formation of shrinkage cavities. For presentation of results chunky castings and bar castings of aluminium alloy and steel have been considered. Cylindrical risers are used in all the cases as it is usually used in metal casting industries. The validity of the results have been tested by comparing the predictions of the present work with the risering curve, for the soundness of a casting of given riser dimensions. These comparisons for the riser design parameters are discussed towards the end of the chapter.

4.1 SOLIDIFICATION ANALYSIS

In Figure 4.1 the process of solidification of a bar casting of aluminium alloy has been shown. The casting size is 85 mm length and 20 mm thick and the riser dimension is 30 mm dia x 40 mm height. It is observed that the solidification begins from the ends of the bar and slowly proceeds towards the riser. This shows that the thermal gradient is appropriate and leads to directional solidification towards the

source of feed metal which is of utmost importance from the point of view of the soundness of the casting. In Fig. 4.1(a) the isotherm of 625°C is plotted. It shows how after a small time mushy zone is formed within the casting. The riser remains liquid at this time which shows that the riser can feed liquid metal to the casting to make up for the shrinkage which occurs as the casting solidifies. Figure 4.1(b) shows the end of solidification. The casting has solidified completely. The isotherm of 525°C is shown. The mushy zone is within the riser which is desirable. It is clear from the figure that the riser dimension chosen in this case would give a sound casting though this is not the optimum riser size. Riser placement is appropriate as the length of the bar is within the maximum feeding distance.

Figure 4.2 and Figure 4.3 show the difference in the solidification rate for bar castings of steel. In the former case only convective heat transfer loss from boundary is considered while in the latter heat loss due to both convection and radiation from the exposed surface of the mould is taken into account. It is observed that the solidification rate is higher due to the enhanced heat transfer when radiation along with convection is taken into account.

4.2 RISER DESIGN AND PLACEMENT

4.2.1 CHOICE OF RISER SIZE

Figures 4.4 to 4.6 show the nature of the solidification process when the riser dimensions are changed. In all these

cases the analysis has been performed on a cubical casting of side 57 mm of aluminium alloy.

In Figure 4.4 the riser is of size 80 mm x 80 mm. It is observed that the solidification starts from the bottom of the casting and the riser is the last part to solidify which is desired. Though a sound casting will be produced with this type of riser, an optimum value of riser size is desired to reduce the cost and extra metal. It is shown later that it is possible to reduce this riser size without affecting the soundness of the casting.

Figure 4.5 shows the effect of changing the riser size. Here, the riser size is 30 mm x 40 mm. It is observed that the solidification rate is such that the riser starts solidifying earlier than that of the casting leaving an isolated liquid region in the casting. Hence the riser cannot feed liquid metal to the casting after its own solidification. This leads to the formation of a shrinkage cavities and hence the riser dimension needs to be modified.

At this stage the riser dimensions of Fig. 4.5 were increased in steps and for each of them the temperature field was calculated and plotted graphically to predict the isolated liquid regions. This procedure was continued until the casting was devoid of isolated liquid regions completely. Here the riser dimensions were noted and it was found out that the optimum riser size was 40 mm x 80 mm (Refer Fig. 4.6) for a 57 mm cubical casting.

4.2.2 RISER PLACEMENT AND OPTIMAL RISER DESIGN PARAMETERS

Figures 4.7 to 4.9 show the importance of the riser placement and its effect on the nature of castings. In all these cases the analysis have been performed for dumbbell shaped castings (cubical parts of 60 mm each and central connection 20 mm x 40 mm) of aluminium alloy.

Figure 4.7 shows the isolated liquid regions during the progress of solidification. Two risers are used, with one at each extreme end of the casting. The riser dimensions are 20 mm dia x 50 mm height. It is seen that after 75 secs. the mushy zone is formed within the riser though some parts of the casting are still in liquid form. So the riser is unsuitable and hence the riser placement should be changed.

Since the intention is to produce a casting devoid of voids or shrinkage cavities, the risers in Fig. 4.7 were both placed at the centre of the cubical portions as shown in Fig. 4.8. Though the size of the isolated liquid region is reduced as compared to the earlier case is reduced, still it is unsuitable for this type of casting.

Now the riser position is kept constant and its size is increased in steps until no isolated liquid regions are found. Two risers each of 50 mm dia x 60 mm height, have been found to be optimum for the casting configuration considered. In the final design therefore the risers may be placed as shown in Fig. 4.9.

The results for these cases have been compared with the findings of earlier works (24) and there is an excellent agreement between them.

4.3 FEEDING DISTANCE

An important aspect of risering is to ensure that the available metal in the riser can be fed to the desired locations within the castings.

To check the accuracy of the predictions from the present model, comparisons were made with known results (24,25) on the maximum feeding distance of a riser.

The general equations for maximum feeding distance (F_{\max}) has been given by Eqn. (2.9) and Eqn. (2.10).

For this aspect of the study only steel bar castings were analysed. Two cases were taken up.


The first case considered is the casting geometry of Fig. 4.2 which shows a steel bar casting with thickness (t) 20 mm and length 90 mm, with the riser dimensions of 30 mm dia x 40 mm height. The maximum feeding distance calculated from Eqn. (2.10) is more than half length of the bar provided in this present case. It is observed that the solidification proceeds from the extreme ends of the bar and there are no isolated regions within the casting. Hence the riser size, placement and feeding distance are appropriate.

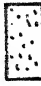
In the second case, for the casting mentioned above the riser dimensions were maintained same along with the


casting thickness, but the casting length was increased to 225 mm as shown in Fig. 4.10 so that half length of the bar exceeds the maximum feeding distance calculated from Eqn.2.10. In the numerical results, isolated liquid regions are observed as expected. Hence the feeding distance should be brought within required limits to prevent the formation of shrinkage cavities.

The results predicted in these cases have been well supported by the available results in literature (24,25) . Thus the present analysis provides a very powerful tool for the optimal design of risers.

The validity of the predictions from the present work upon the soundness of castings are compared with those of risering curve in Fig. 4.11. For the situations considered in Figs. 4.2 (Case I) and 4.10 (Case II). The volume ratio (V_r/V_c) and freezing ratio $(A/V)_c/(A/V)_r$ have been calculated for these casting configurations and the points corresponding to these values have been placed in relation to the risering curve. It is observed that the point for case I falls in the zone of sound castings, while that for case II does not. These observations are in good agreement with the predictions of the present work.

 Liquid
 GE 625°C

 Mushy
 525°C - 624°C

 Solid
 LT 525°C

Solidification Time in sec.

(a) 45

(b) 225

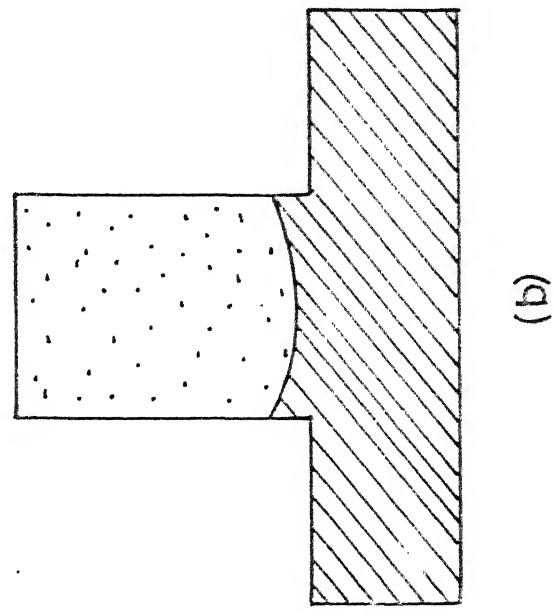
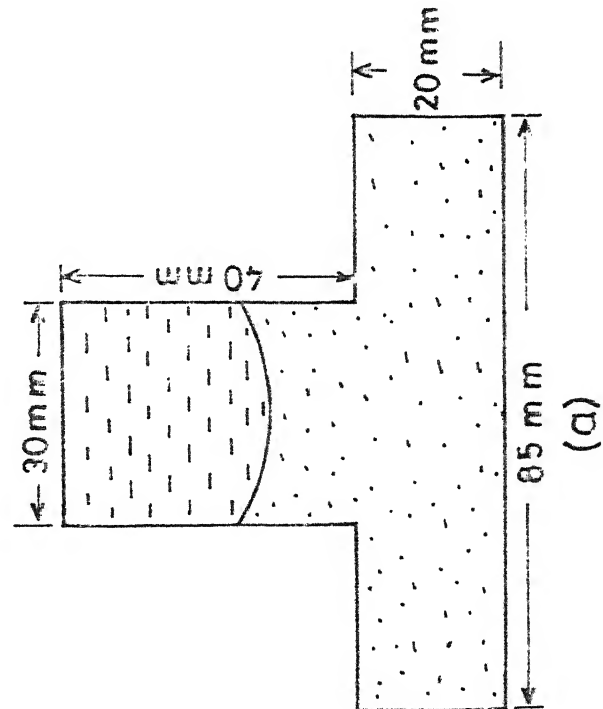


Fig. 4.1 Solidification of a Bar Casting of Aluminium Alloy (92.5% Al, 3% Cu, 4.5% Ni)

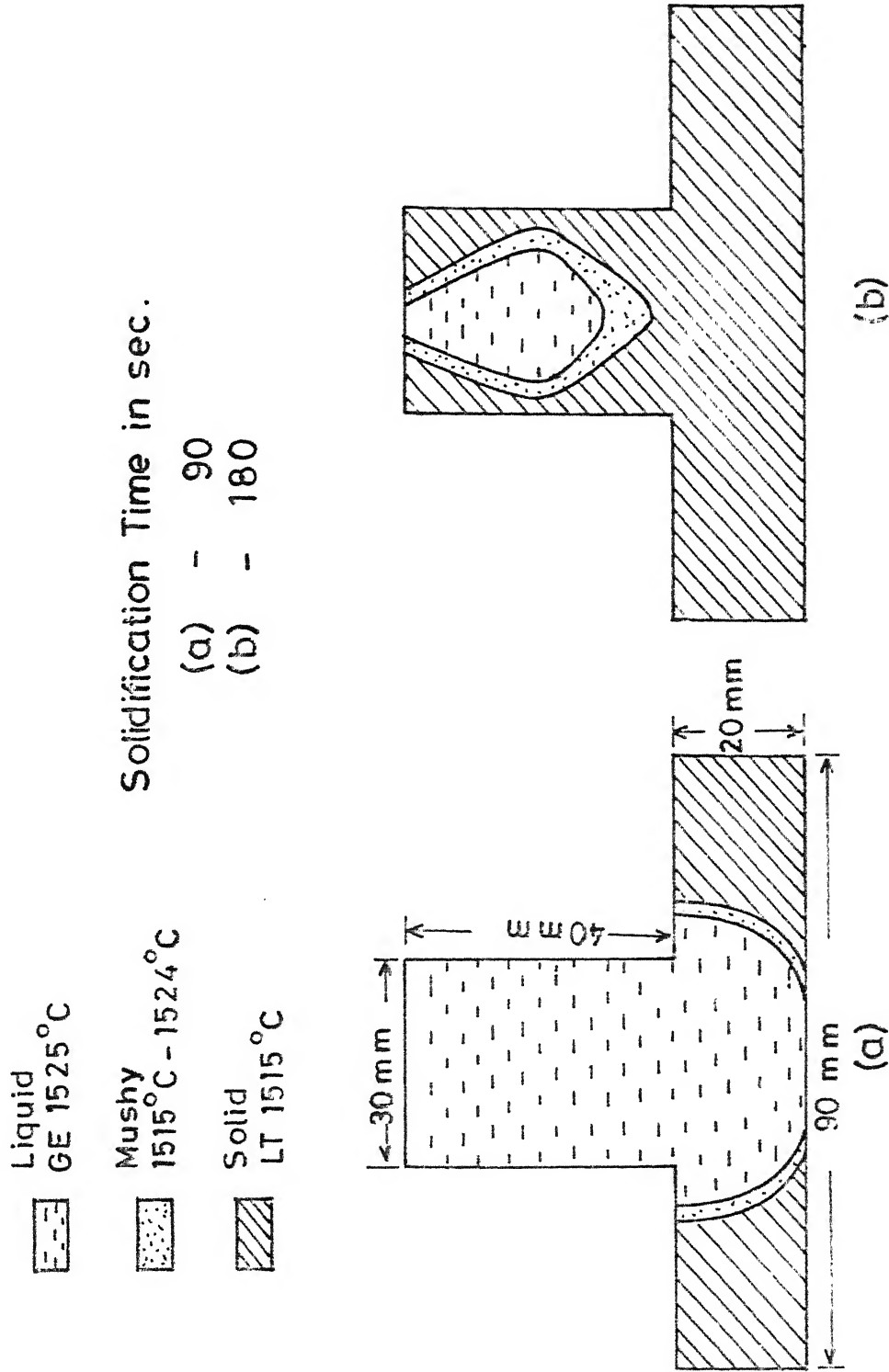


Fig. 4.2 Solidification of a Bar Casting of 0.15% Carbon Steel for Convective Heat Loss from the Boundary. No Centreline Shrinkage Area when Bar of Length Twice the Maximum Feeding Distance of Riser.

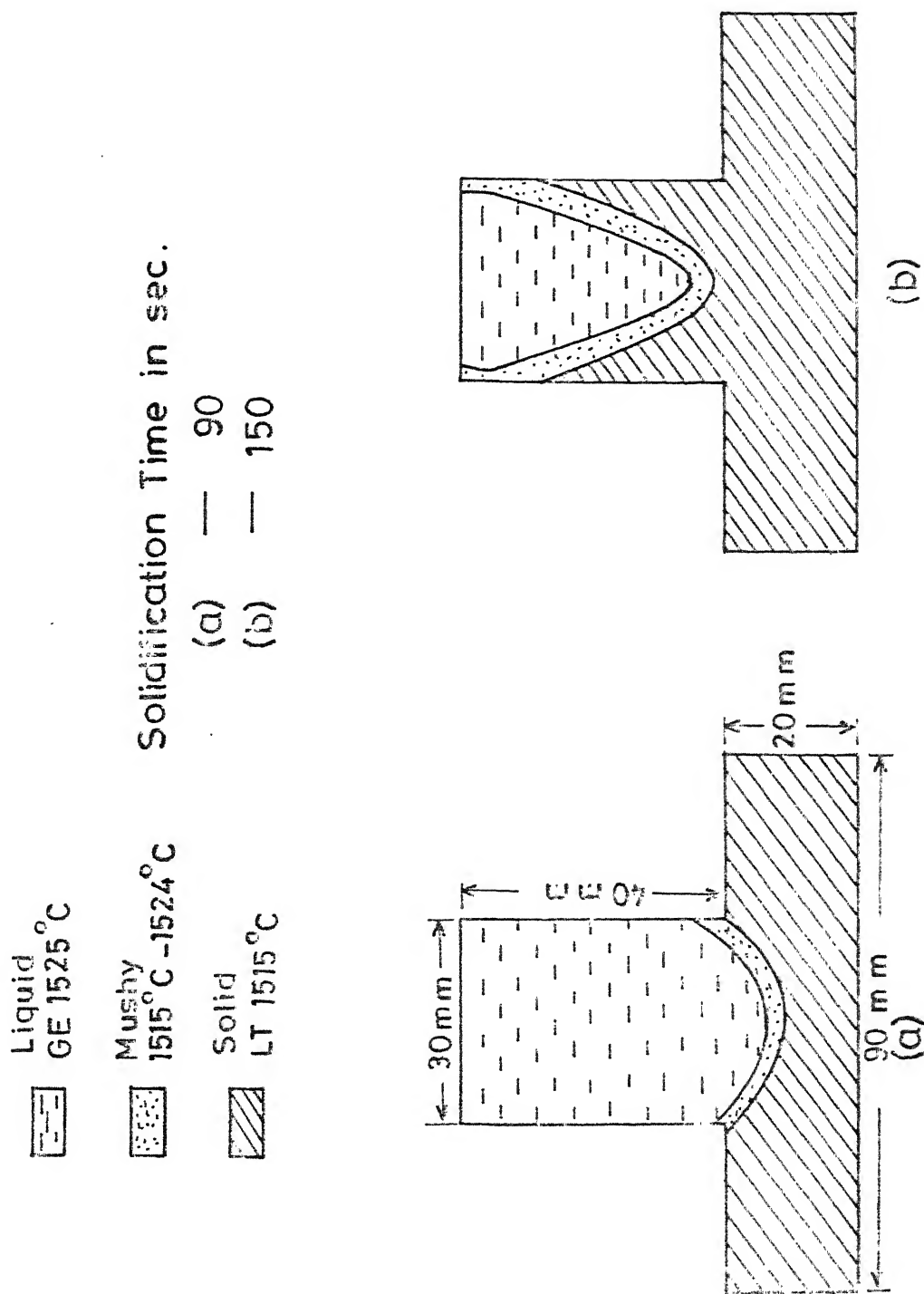
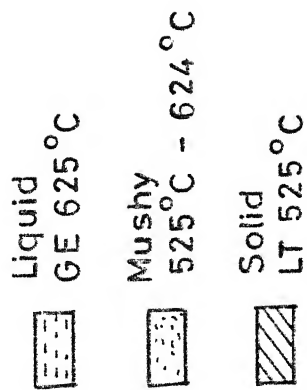


Fig. 4.3 Solidification of a Bar Casting of 0.15 % Carbon Steel for Convective and Radiative Heat Loss from the Boundary.



Solidification Time in sec.

- | | |
|-----|-------|
| (a) | — 90 |
| (b) | — 480 |
| (c) | — 600 |

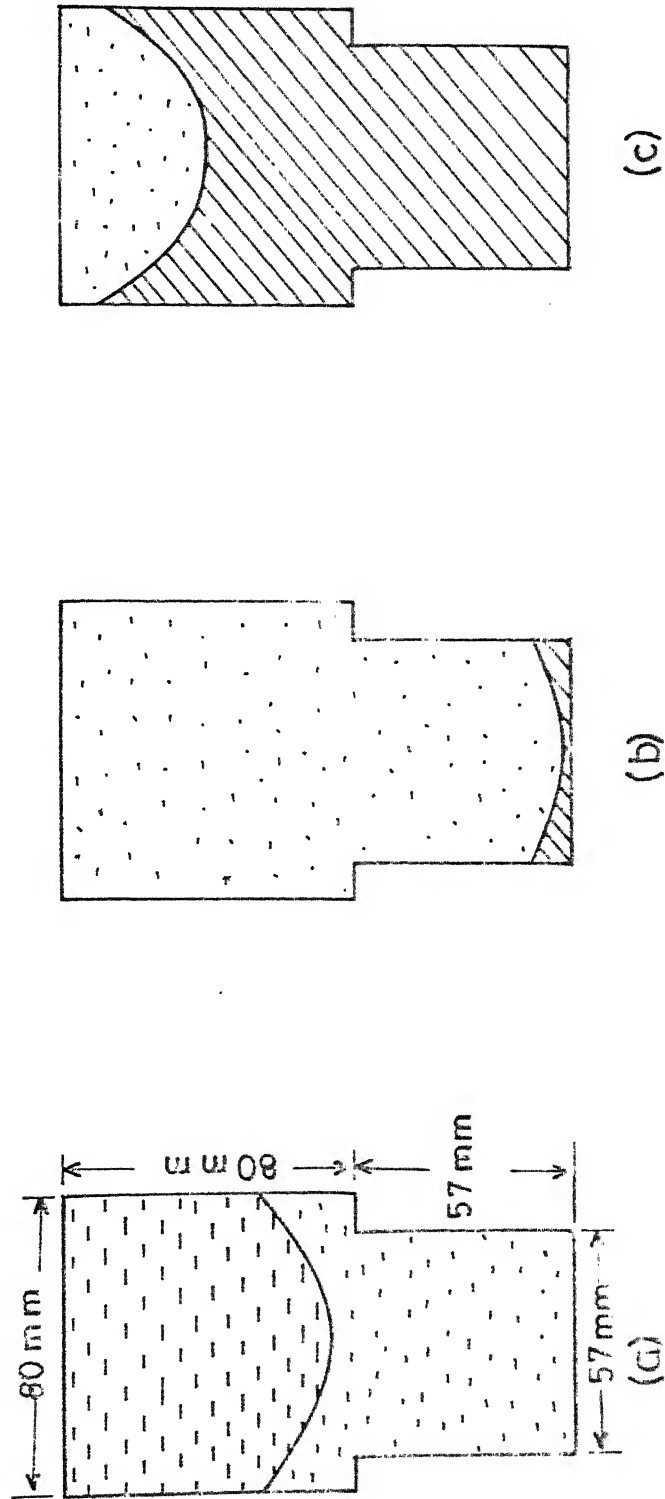


Fig. 4.4 Riser of a Cube Casting of Aluminium Alloy (92.5% Al, 3% Cu, 4.5% Ni) Proportionate Riser Used.

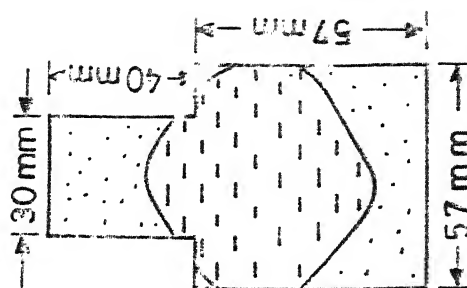
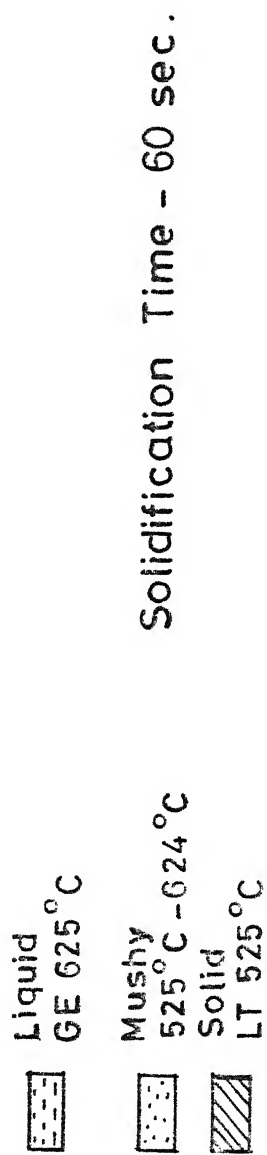


Fig. 4.5 Riser of a Cube Casting of Aluminium Alloy (92.5% Al, 3% Cu, 4.5% Ni). Disproportionate Riser Used.

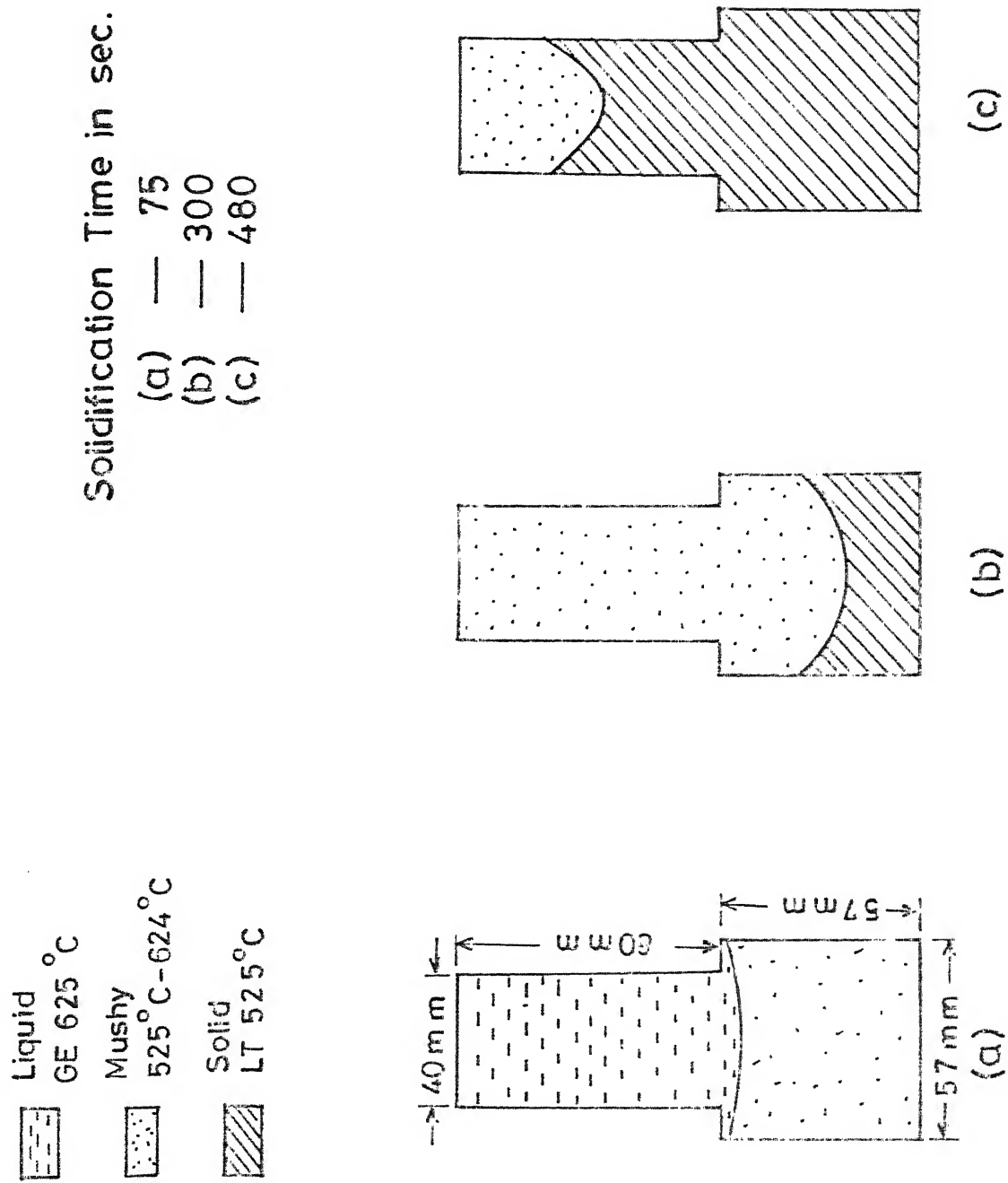
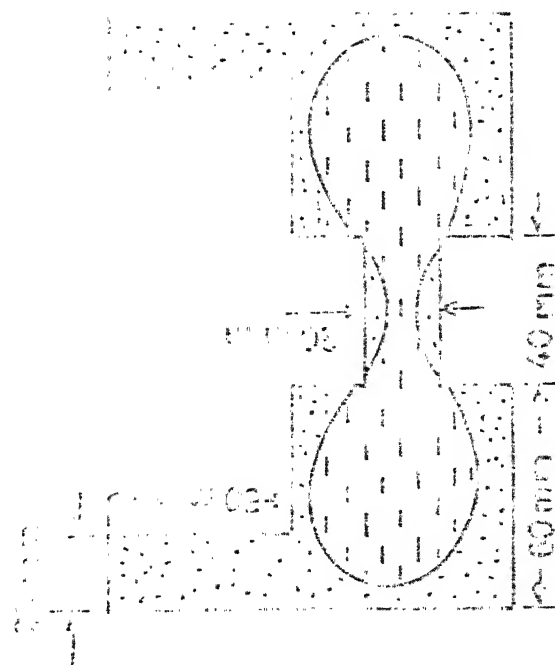
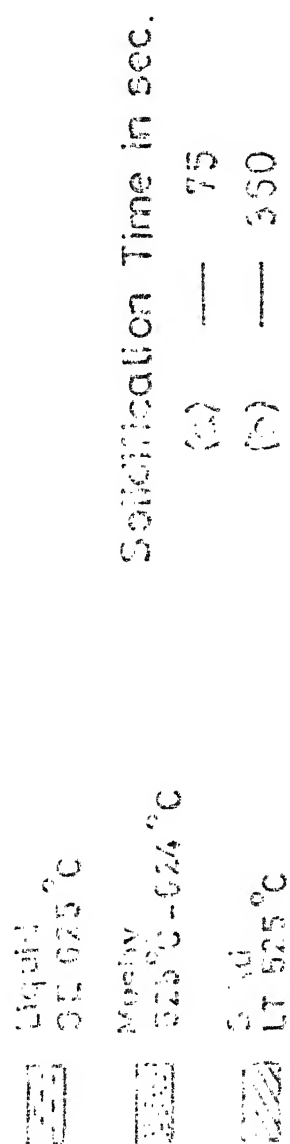
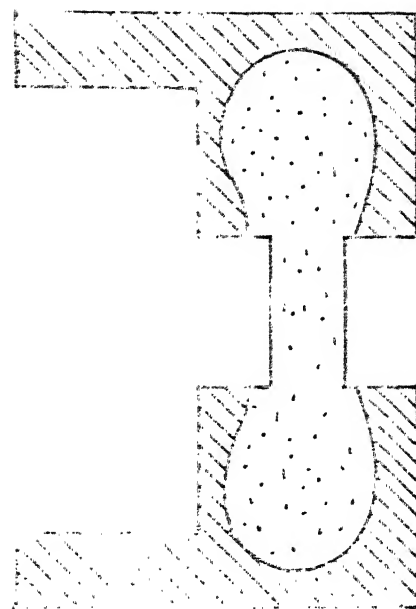


Fig.4.6 Riser of a Cube Casting of Aluminium Alloy (92.5% Al, 3% Cu, 4.5% Ni). Modified Optimum Riser Used.



(a)



(b)

Fig. 4.7 Riserings of a Dumbbell Shaped Casting of Aluminium Alloy (92.5% Al, 3% Cu, 4.5% Ni) with Two Risers, One at Each End of the Casting. Isolated Liquid Region Seen.

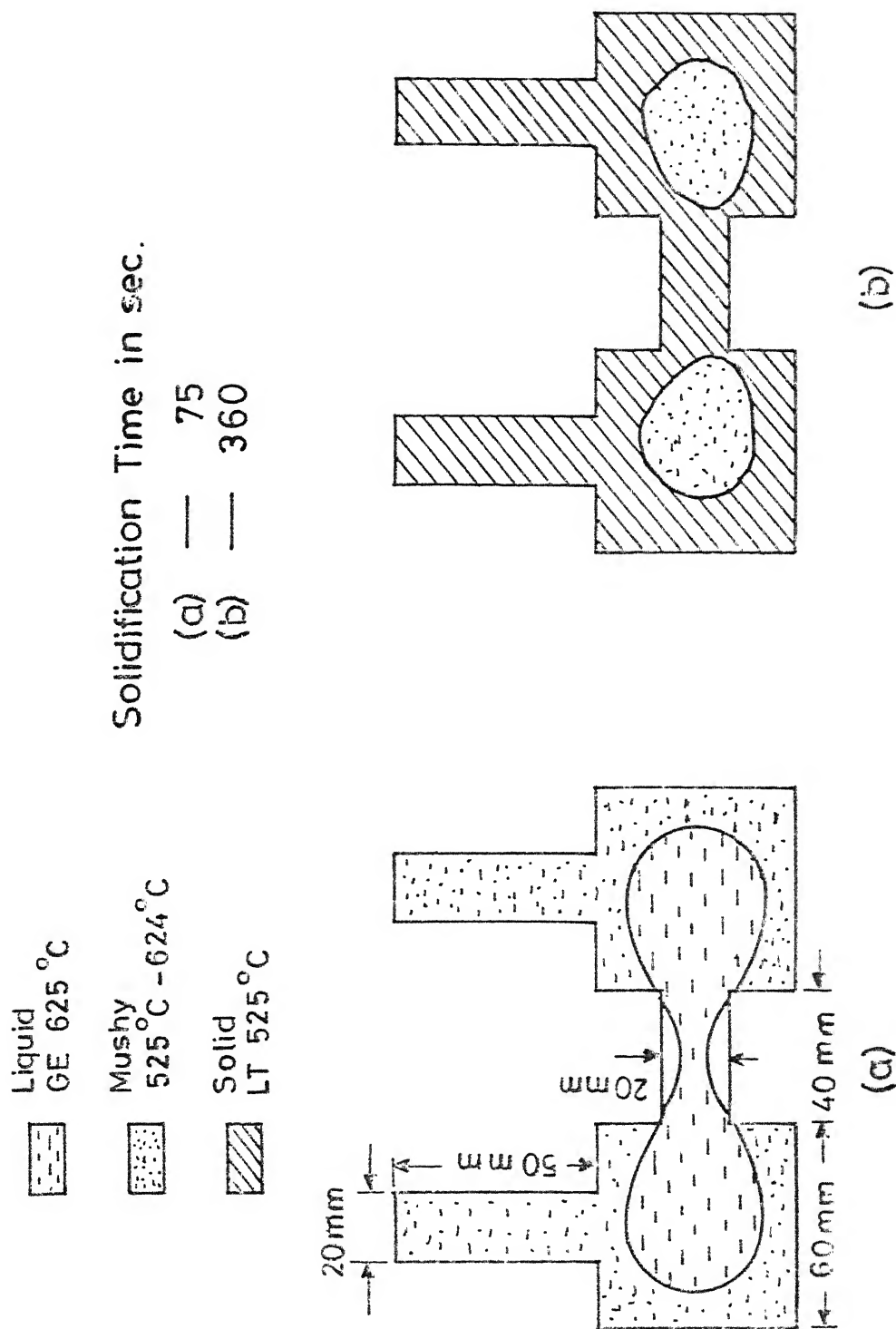


Fig. 4.8 Riser of a Dumbbell Shaped Casting of Aluminum Alloy (92.5% Al, 3% Cu, 4.5% Ni) with Two Riser One Each at the Centre of Each Casting. Isolated Liquid Region Seen.

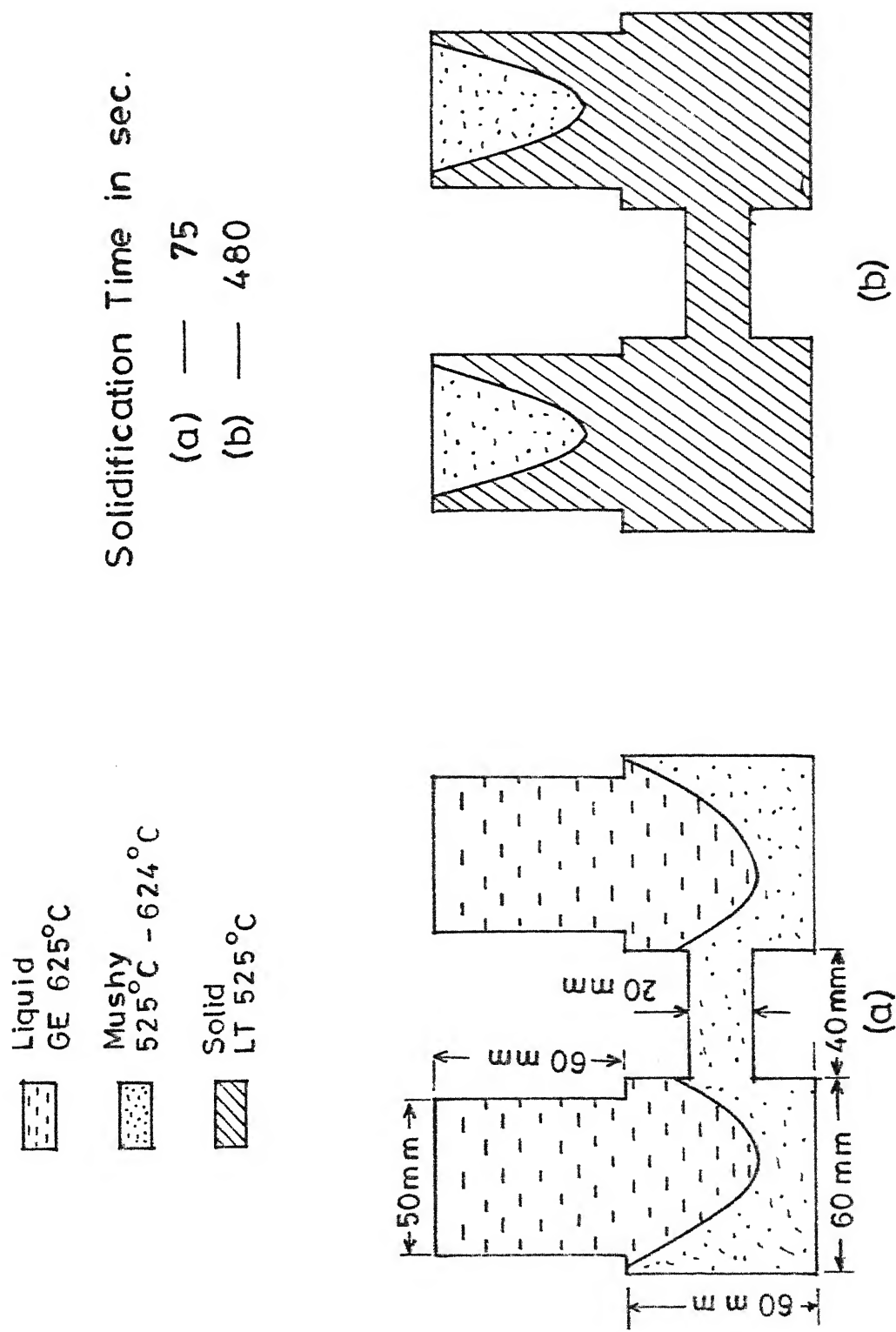


Fig. 4.9 Riserling of a Dumbbell Shaped Casting of Aluminium Alloy (92.5% Al, 3% Cu, 4.5% Ni) Two Proportionate Risers One Each at the Centre of Each Casting. No Isolated Liquid Region Seen.

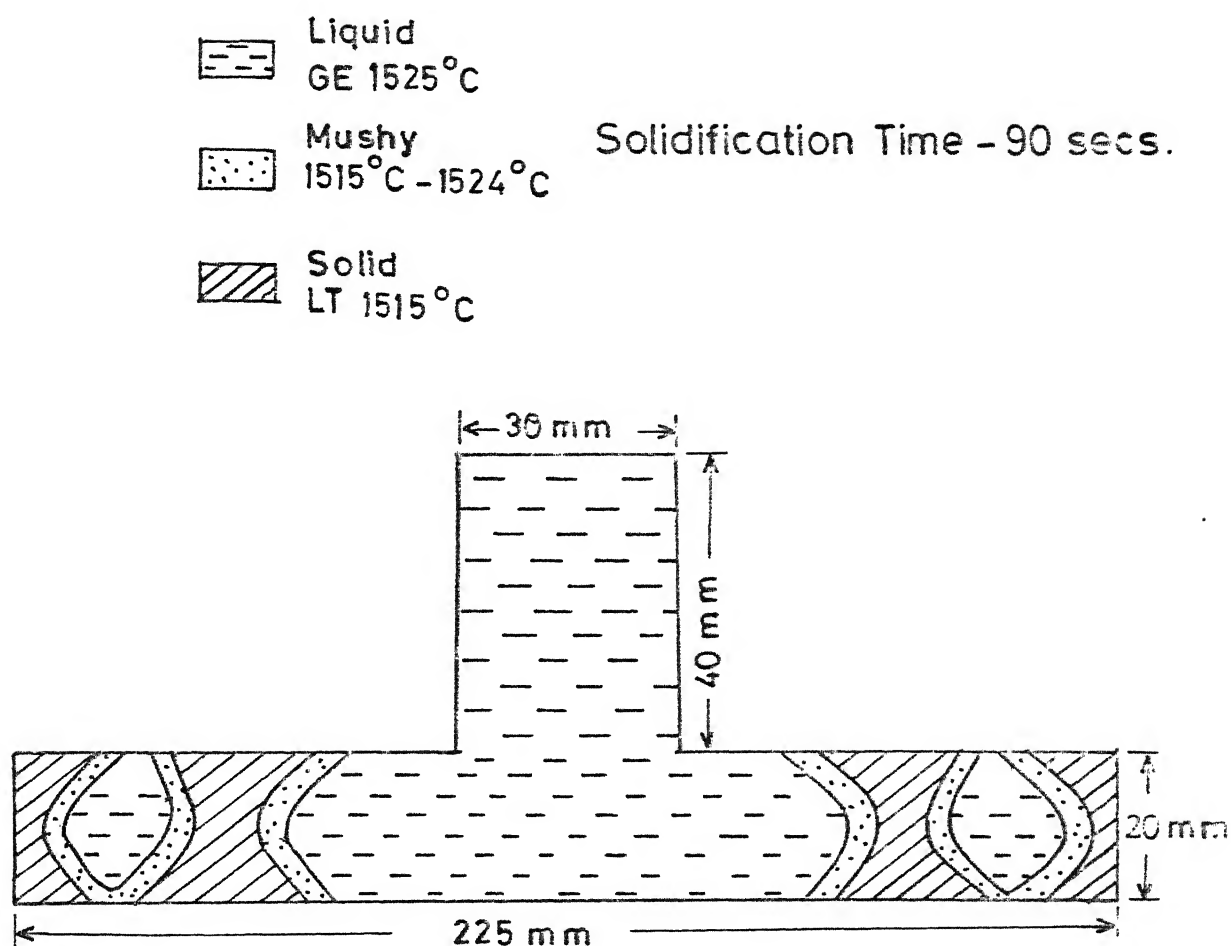


Fig. 4.10 Solidification of a Bar Casting of 0.15 % Carbon Steel. Centreline Shrinkage Areas Seen When Bar Length Greater Than Twice the Maximum Feeding Distance.

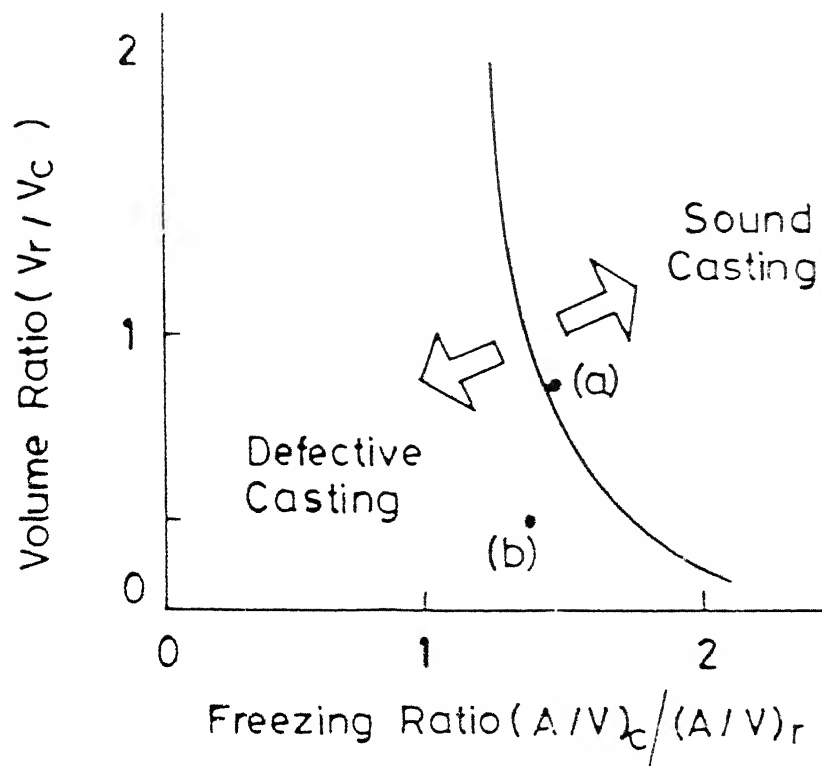


Fig. 4.11 Comparison of Present Result with Typical Riser Curve. Point (a) corresponds to Fig. 4.2. Point (b) corresponds to Fig 4.10.

CHAPTER 5

CONCLUSIONS AND SUGGESTIONS

5.1 CONCLUSIONS

(1) For the particular type of castings analysed, changes in the riser dimensions and riser placement have a large effect in the soundness of the casting.

(2) The present riser design procedure can give significant improvements in true casting yield.

5.2 SUGGESTIONS FOR FUTURE WORK

(1) The present problem can be easily extended to more practical situations of three dimensional geometry castings.

(2) The phenomenon of natural convection within the liquid metal can be looked into and the enhancement of heat transfer due to this phenomenon can be precisely modelled.

(3) Detailed variations in thermal properties can be considered and the analysis can be performed for various alloy metals.

(4) Mass transfer aspects of alloy solidification and detailed flow considerations within the mushy zone through a porous medium approach, can be included.

REFERENCES

1. H.S. Carslaw and J.C. Jaeger, Conduction of Heat in Solids, 2nd edn., Oxford University Press, 1959.
2. S.H. Cho and J.E. Sunderland, 'Heat Conduction Problems with Melting or Freezing', J. Heat Transfer, 91, 421-426 (1969).
3. S.H. Chan, D.H. Cho and G. Kocamustafaogullari, 'Melting and Solidification with Internal Radiative Transfer - a Generalized Phase Change Model,' Int. J. Heat Mass Transfer, 26, 621-633 (1983).
4. J. Szekely and P.S. Chabra, 'The Effects of Natural Convection on the Shape and Movement of Melt-Solid Interface in the Controlled Solidification', Met. Trans. B, 1, 1195-1203 (1970).
5. A. Gadgil and D. Gobin, 'Analysis of 2-D Melting in Rectangular Enclosures in Presence of Convection', J. Heat Transfer, 25, 20-26 (1984).
6. P.G. Kroeger and Ostrach, 'The Solution of a 2-D Freezing Problem including Convection', Int. J. Heat Mass Transfer, 1974, Vol. 17, p. 1191.
7. J. Szekely and V. Stanek, 'Natural Convection Transients and their Effects of Unidirectional Solidification', Metall. Trans., 1970, Vol. 1, p. 2243.
8. E.M. Sparrow, S.V. Patankar, S. Ramadyani, 'Analysis of Melting in the Presence of Natural Convection in the Melt Region', ASME J. Heat Transfer, 1977, Vol. 99, p. 520.
9. N. Ramachandran, J.P. Gupta and Y. Jaluria, '2-D Solidification with Natural Convection in the Melt and Convective and Radiative Boundary Conditions', Numerical Heat Transfer, 1981, Vol. 4, p. 469.
10. Jaisuk Yoo and B. Rubinsky, 'A Finite Element Method for the Study of Solidification Processes in the Presence of Natural Convection', Int. J. Num. Meth.in Engg., 1970, Vol. 2, p. 1785.
11. J.A. Shekar, S. Kou and R. Mehrabian, 'Heat Flow Model for Surface Melting and Solidification of an Alloy', Metall. Trans. A, 1983, Vol. 14A, p. 1169.

12. S.C. Hsu, S. Chakravorty and R. Mehrabian, 'Metall. Trans. B, 1978,
13. W.D. Murray and F. Landis, 'Trans. ASME, 1959, Vol. 81, p. 106.
14. N. Chvorinov, 'Theory of Solidification of Castings', Giesserei, Vol. 27, p. 177 (1940).
15. J.B. Caine, 'A Theoretical Approach to the Problem of Dimensioning Risers', p. 492, AFS Trans., 1948.
16. H.F. Bishop, 'A Simplified Method for Determining Riser Dimensions', p. 724, AFS Trans., 1955.
17. Harish D. Merchant, 'Dimensioning of Sand Casting Risers', pp. 93-104, AFS Trans., Vol. 67, 1959.
18. T.S. Prasanna Kumar et.al., 'Finite Element Formulations for Estimating Feeding Efficiency Factors', pp. 789-799, AFS Trans., 1985.
19. I. Imafuku, K. Chijiwa, 'A Mathematical Model for Shrinkage Cavity Prediction in Steel Castings', p. 527, AFS Trans., 1983.
20. I. Imafuku, K. Chijiwa, 'Application and Consideration of the Shrinkage Cavity Prediction Method', p. 463, AFS Trans., 1983.
21. S. Abis, 'Numerical Simulation of Solidification in an Aluminium Casting', Metall. Trans. B, 1986, Vol. 17B, p. 209.
22. G.L. Shekar, 'Computer Aided Design of Riser for Sand Castings', M.Tech. Thesis, Department of Mechanical Engineering, I.I.T. Kanpur, January 1988.
23. B.M. Irons, 'A Frontal Solution Program for Finite Element Analysis', Int. J. Num. Meth. in Engg., Vol. 2, 1970.
24. M.C. Flemings, 'Solidification Processing', McGraw-Hill, 1974.
25. W.S. Pellini, 'Factors which Determine Riser Adequacy and Feeding Range', p. 61, AFS Trans., pp. 61-80.

